TECHNICAL UNIVERSITY OF LIBEREC
Faculty of Mechanical Engineering

Calibration of piezoelectric film sensors for the cavitation aggressiveness measurement

Master Thesis

Study programme: N2301 Mechanical Engineering
Study branch: Machines and Equipment Design

Author: **Linn Htet**
Thesis Supervisors: Ing. Miloš Müller, Ph.D.
Department of Power Engineering Equipment

Liberec 2021

TECHNICAL UNIVERSITY OF LIBEREC
Faculty of Mechanical Engineering

Master Thesis Assignment Form

Calibration of piezoelectric film sensors for the cavitation aggressiveness measurement

Name and surname: **Linn Htet**
Identification number: S17000378
Study programme: N2301 Mechanical Engineering
Study branch: Machines and Equipment Design
Assigning department: Department of Power Engineering Equipment
Academic year: **2019/2020**

Rules for Elaboration:

- A review of methods used for the calibration of piezoelectric film sensors
- The selection of an appropriate method for the calibration of piezoelectric film sensors used for the measurement of the cavitation aggressiveness
- The design of an experimental assembly for the realization the selected calibration method
- The calibration of piezoelectric film sensors with the selected calibration method
- Application of the sensors calibrated by the selected method to the measurement of the aggressiveness of an ultrasonic cavitation field
- The critical evaluation of the results obtained by the selected calibration method
- The recommendations for the application of the selected calibration method

Scope of Graphic Work: 10
Scope of Report: 50
Thesis Form: printed/electronic
Thesis Language: English

List of Specialised Literature:

1. KIM, Ki-Han, Georges CHAHINE, Jean-Pierre FRANC a Ayat KARIMI. *Advanced experimental and numerical techniques for cavitation erosion prediction*. Dordrecht: Springer, [2014]. Fluid mechanics and its applications, v. 106.
2. FRANC, Jean-Pierre a Jean-Marie MICHEL. *Fundamentals of cavitation*. Boston: Kluwer Academic Publishers, c2004. ISBN 1402022328.
3. BRENNEN, Christopher E. *Cavitation and bubble dynamics*. New York: Cambridge University Press, c2014. ISBN 978-1-107-64476-2.
4. SOYAMA, Hitoshi, MOMMA Takahiro, LICHTAROWICZ Andrzej and Edward WILLIAMS. *A New Calibration Method for Dynamically Loaded Transducers and Its Application to Cavitation Impact Measurement*. Journal of Fluids Engineering. 1998, 120(4). 10.1115/1.2820728.

Thesis Supervisors: Ing. Miloš Müller, Ph.D.
Department of Power Engineering Equipment

Date of Thesis Assignment: November 1, 2019
Date of Thesis Submission: June 7, 2021

L.S.

prof. Dr. Ing. Petr Lenfeld
Dean

doc. Ing. Petra Dančová, Ph.D.
Head of Department

Liberec February 14, 2020

Declaration

I hereby certify, I, myself, have written my master thesis as an original and primary work using the literature listed below and consulting it with my thesis supervisor and my thesis counsellor.

I acknowledge that my bachelor master thesis is fully governed by Act No. 121/2000 Coll., the Copyright Act, in particular Article 60 – School Work.

I acknowledge that the Technical University of Liberec does not infringe my copyrights by using my master thesis for internal purposes of the Technical University of Liberec.

I am aware of my obligation to inform the Technical University of Liberec on having used or granted license to use the results of my master thesis; in such a case the Technical University of Liberec may require reimbursement of the costs incurred for creating the result up to their actual amount.

At the same time, I honestly declare that the text of the printed version of my master thesis is identical with the text of the electronic version up- loaded into the IS/STAG.

I acknowledge that the Technical University of Liberec will make my master thesis public in accordance with paragraph 47b of Act No. 111/1998 Coll., on Higher Education Institutions and on Amendment to Other Acts (the Higher Education Act), as amended.

I am aware of the consequences which may under the Higher Education Act result from a breach of this declaration.

June 7, 2021 Linn Htet

ABSTRACT

In the introductory part of the thesis, a brief explanation about the dynamic of bubble cavitation in homogenous and heterogeneous nucleation, pressure domain bubble growth and collapse. A review of methods used for the calibration of piezoelectric film sensors was elaborated to select the most appropriate method for the cavitation aggressiveness measurement. Regarding the sort pulse duration, the pencil-lead breaking method was selected. The test using the drop ball method was used performed for the comparison. To realize the calibration method an experimental assembly for the pencil-lead breaking method was designed and manufactured. Two kinds of sensors were tested using the pencil lead breaking method and the drop ball method. Pencil-lead breaking calibration two different hardness of 2mm pencil lead with two protruding lengths. The resulting constants are directly applicable to any measurements using tested PVDF films. The applicability of the pencil-lead breaking method was discussed resulting in the extension and modification of the experiment.

ACKNOLDEGEMENTS

First of all, I would like to express my deepest gratitude to my supervisor, Ing. Miloš Müller, Ph.D., whose expertise, immensely support, and continuous guidance has greatly helped me throughout this thesis study. I dedicate this work to my family, Daw Aye Aye Thein and U Sett Htun, whose unwavering love and encouragement in all things. Likewise, I want to express gratitude toward U Linn Thant's Family and Daw Sabe Soe for who gave unconditional support while I was in medical issue.

This study was supported as part of the project "*interaction of cavitation bubbles with surfaces*" with the support of the Specific University Research Grant by the Technical University of Liberec.

Table of Contents

List of figures

List of tables & Appendix

List of Symbols

Roman Letter

Symbol	Description	unit
C_P	Specific heat at constant pressure	[KJ/kg K]
C_s	capacitance of the sensor	[F]
D	electric displacement	[C]
d	piezoelectric strain charge constant	[C/N]
E	electric field	[V/m]
F_{max}	maximum force	[N]
F_{avg}	average force	[N]
g	gravitational acceleration	[m^2/s]
h	height	[m]
M	moment	[N/m]
m	mass	[Kg]
P	Pressure	[Pa]
P_a	acoustic pressure amplitude	[Pa]
P_B	Bubble Pressure	[Pa]
P_{g0}	Pressure of the gas inside the bubble at initial state	[Pa]
P_l	Liquid Pressure	[Pa]
P_∞	ambient pressure	[Pa]
P_v	Vapor Pressure	[Pa]
q	charge	[C]
R	Bubble Radius	[m]
$\dot{R}$	First order derivative of bubble radius with respect to time	[m/s]
$\ddot{R}$	Second order derivative of bubble radius with respect to time	[m/s^2]
S	surface tension	[N/m]
s	electric compliance	[$m^{2/N}$]
T	mechanical Strain	[-]

t	time	[s]
T	Temperature	[K]
T_∞	reference Temperature	[K]
V	volume	[m^3]
Vs	Voltage generated by the sensor	[V]
v_j	microjet velocity	[m/s]
v	velocity	[m/s]
U_∞	reference velocity	[m/s]
σij	Stress tensor	[N]
i, j, k	Indices	[-]
u_i	Velocity vector	[m/s]

Greek Letters

Symbol	Description	unit
ρ	density	[kg/m^3]
σ	Cavitation number	[-]
σ_i	Cavitation inception number	[-]
ν	Kinematic viscosity	[m^2/s]
τ	duration of time	[s]
ε	dielectric constant	[F/m]

1. INTRODUCTION

Cavitation is can be defined as a collection of effects connected with activities of macroscopic cavities noted as bubbles. These bubbles can cause severe damage to the surfaces of hydrodynamic machines. For the quantification of the bubble impact magnitude different sensors are used. The requirements to the sensors are given by the cavitation flow properties which include the high frequency response and mechanical resistance. The PVDF film sensors appear to be suitable for this application. The problem which originates from the PVDF film sensors application is the missing relation between the produced voltage and the impact force. This is provided by calibration. To obtain a good agreement between the real cavitation impact and the calibration impact the same time duration between these two should be reached. Based on this a review of calibration methods is elaborated. Based on the review an appropriate calibration method is selected and an experimental setup is designed and assembled. The calibration results are evaluated and compared with the other calibration method.

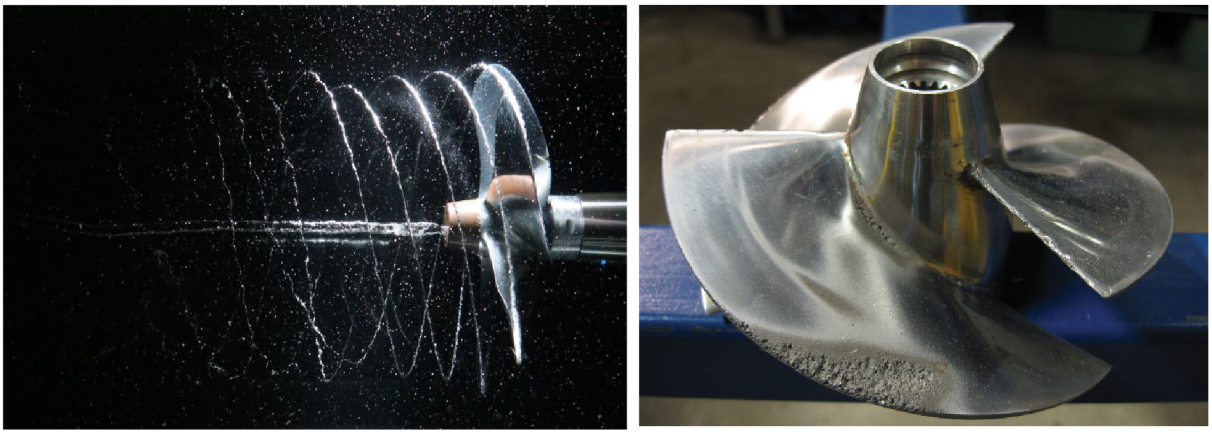

Figure 1-1 Cavitation at boat propeller blade and erosive effect

2. DYNAMIC OF CAVITATION

In this chapter a brief explanation of forming of bubble nuclei, bubble growth and collapse is given.

2.1 Description of Cavitation

The term 'cavitation' can be referred to the formation of cavities bubbles inside a homogenous liquid medium by the pressure reduction beyond its vapor pressure whereas liquid cohesion can no longer be endured. That can occur both in static and dynamic conditions [1].

2.2 Cavitation Behavior

Cavitation bubbles are voids formed in homogenous medium during phase changing from liquid to vapor state. The behavior of cavitation can be described according to Figure (2.1) typical in water phase diagram, where are pressure, *P*, temperature, *T*, and specific volume, *V*. Liquid phase to vapor phase can be changed by two methods; from point 1to 2 by depressurizing called cavitation or, by increasing temperature point 1 to 3 called boiling.

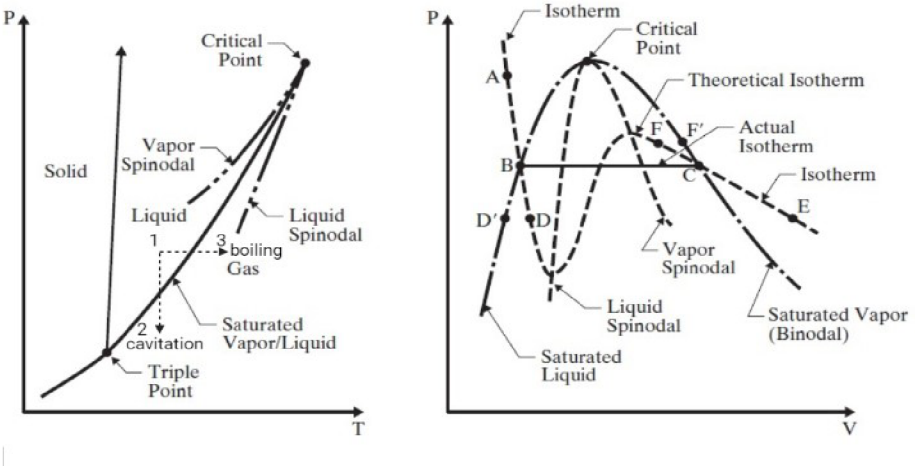

Figure 2-1 Typical Phase diagrams [3]

The point where solid, liquid and vapor states coexist alternatively in stable state is called *triple point*. In the critical point is liquid and vapor phases merge into a single-phase. Beyond the pressure of the critical point, the phase is known as a supercritical fluid. Vapor and liquid phases coexisting two limiting forms of a single amorphous called *saturated vapor/liquid*, one of which can be obtained by isothermal volumetric changes from point B to C. The Saturated Vapor/ Liquid line can be extended from triple point to critical point also called binodal line. Line joining minima of theoretical isotherm to the critical point is called liquid spinodal and maxima to the critical point called vapor spinodal. Between binodal and spinodal regions are metastable phase. In interest of cavitation, a pure liquid state from point A is depressurized below to point B. If no nucleation sites are present depressurizing continue to metastable region point D. Pressure difference between B, saturated vapor pressure, P_v and pressure P at point D where rupture occurs at constant temperature is the magnitude tensile strength of the liquid medium [2] [3].

2.3 Classification of Cavitation

Cavitation can be classified into two major groups base on its occurrence.

Due to **Tension** in the liquid, we can observe the following cavitation types:

1. *Acoustic Cavitation*: produced by sound waves in a liquid due to pressure variations.
2. *Hydrodynamic Cavitation*: produced by pressure variations in flowing fluid due to the geometry of the system.

Due to **Energy Deposit** in the liquid, we can observe the following cavitation types:

1. *Optic cavitation*: produced by photons of high-intensity light (laser) rupturing in a liquid
2. *Particle cavitation*: produce by any other type of high energy elementary particle, e.g., proton, rupturing a liquid in a bubble chamber.

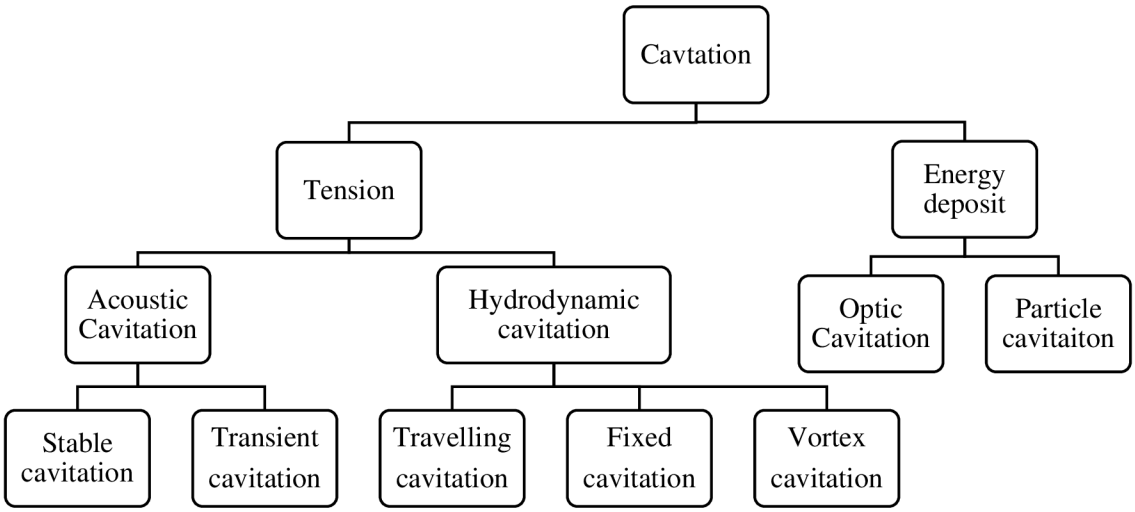

Figure 2-2 Classification scheme for different types of cavitation [6]

2.3.1 Acoustic Cavitation

In a non-flowing system, ambient pressure, P_{∞}, can be varied by subjecting sound waves through the liquid. If the amplitude of the pressure, P_a, variations is great enough to bring the pressure locally down to, or below vapor pressure as the sound cycle traversing the liquid, any minute cavities or bubbles will in motion of compression and expansion Figure (2.3). There are two distinct types of bubble motions possible;

1. *Stable cavities*: Mega sonic frequencies, 700 to 1000 Hz produce stable cavities that can continue oscillating for many cycles of the acoustic pressure, around some equilibrium size even non- linear. They are small, less time to grow, in less aggressive to produce surface damage than transient cavitation.
2. *Transient cavities*: Ultrasonic frequencies, 20 to 350 kHz produce transient cavities. They generally collapsed within one cycle. During this cycle, they expand at least two

times to a radii, many times larger than their original size. After the collapse bubble structures disintegrating into smaller bubbles [4] [5].

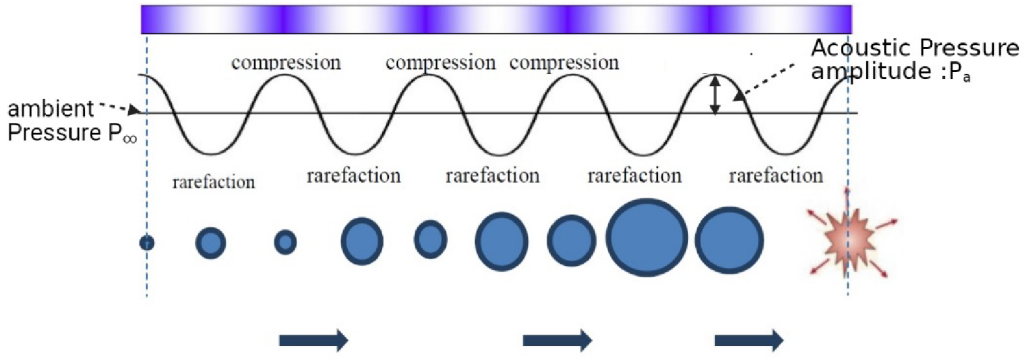

Figure 2-3 Acoustic Cavitation mechanism[5]

2.3.2 Hydrodynamic cavitation

In the Flowing system, the liquid velocity varies locally due to some discontinuities like surface roughness, geometry, etc. and at the point of highest velocity, low pressures induced cavities occur. Hydrodynamic cavitation further can be classified into three types**:**

1. *Travelling Cavitation*: cavities or bubbles form in the liquid and grow travel along with the motion of the liquid as they expand and subsequently collapse.
2. *Fixed cavitation*: occurs when a cavity or pocket attached to the rigid boundary of an immersed body, and remain fixed in position in an unsteady state.
3. *Vortex cavitation*: occurs in cores of vortices which form in regions of high shear and blade tips of ship's propellers also called tip cavitation [6].

2.4 Nucleation

Nucleation is the process at the beginning of the phase change process. There are primarily two types of nucleation:

2.4.1 Homogenous Nucleation

Homogenous nuclei are formed in the pure liquid bulk where without contaminations and gas. In pure liquid, surface tension is a macroscopic manifestation of the intermolecular force to hold molecules together and prevent the formation of large vacancies between the molecules. It can be express by the following equation:

$$P_B - P_l = \frac{2S}{R} \qquad (2.1)$$

Where P_B is the interior bubble pressure, P is liquid pressure, R is the radius of bubble, S is the surface tension. If the temperature is uniform, the bubble contains only vapor, the interior pressure of the bubble P_B will be the same as the saturated vapor pressure $P_{v(T)}$. The equation (2.1) becomes;

$$P_B = P_v - \frac{2S}{R} \qquad (2.2)$$

For equilibrium of the equation (2.2), liquid pressure must be less than the saturated vapor pressure $P_{v(T)}$. If the exterior liquid pressure is maintained slightly lower than $P_v - \frac{2S}{R}$, bubble will grow and grooving radius, R will increase with excess in pressure and the liquid will be ruptured. The tensile strength of the liquid, ΔP_c, pressure difference between the bubble interior and bubble exterior, is reached when the vacancy reaches critical radius R_c. The tensile strength of the liquid can be given by the following equation [3].

$$\Delta P_C = \frac{2S}{R_c} \qquad (2.3)$$

2.4.2 Heterogenous Nucleation

In the case of the heterogenous nucleation: the nuclei formed at submerged walls of the container or at the suspended particles [7]. The relation between solid and liquid interface is represented by the contact angle θ as shown in Figure (2.4). In the case of a flat hydrophobic surface, tensile strength is given by the following equation:

$$\Delta P_C = \frac{2S\sin\theta}{R_c} \qquad (2.4)$$

where R is the maximum dimension of the void. The tensile strength approach to zero when θ⟶π. For the hydrophilic surface, the tensile strength is comparable with the one for homogeneous nucleation cavity case. In a microscopic scale, surfaces are rough. Like in conical (c), the half angle of vertex cavity is denoted as α, that is zero tensile strength $\theta = \alpha + \pi/2 = 90°$. When $\theta > \alpha + \pi/2$ vapor pocket will be driven to fill the cavity at a pressure above the vapor pressure.

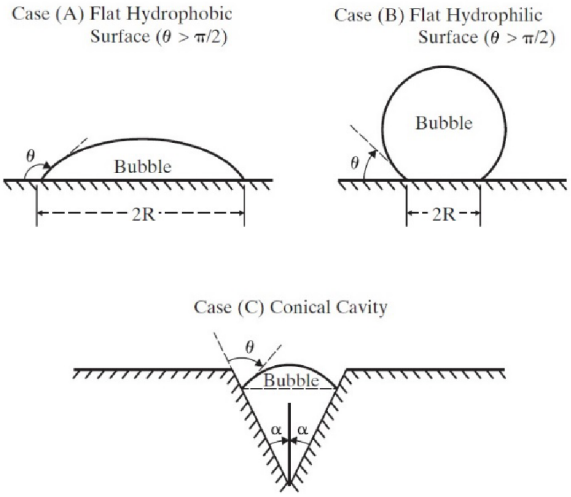

Figure 2-4 Modes of Heterogenous nucleation

2.5 Cavitation Inception in Flowing Liquids

In this section will be consider as a single-phase, inviscid steady flow of Newtonian liquid where $u_i(x_i)$ is the velocity field, $P(x_i)$ pressure and ρ_L constant liquid density and, P_∞ and U_∞ are uniform upstream reference pressure and velocity. The magnitude of the lowest pressure at xi* location in the single-phase flow is given by the minimum value of the coefficient of pressure by the following equation

$$C_{p(xi^*)} = \frac{2(P_{(xi^*)} - P_v)}{\rho U_\infty^2} \qquad (2.5)$$

When either the flow velocity is increased or the pressure decreased, at some point, the flow approaches the vapor pressure, P_v at a reference temperature, T_∞. The potential of cavitation can be

determined by means of cavitation number σ

$$\sigma = \frac{2(P_\infty - P_v)_{T\infty}}{\rho U_\infty^2} \qquad (2.6)$$

In idealized inviscid flow, $C_{p(xi^*)}$ is only dependent on the geometry of the flow boundaries and note that it is a negative number, $-C_{p(xi^*)}$ become positive number. In rough approximation, cavitation inception can be considered to occur at vapor pressure so

$$\sigma_i = -C_{p(xi^*)} \qquad (2.7)$$

Unfortunately, many factors can cause the actual value of σ_i will radially depart from $-C_{p(xi^*)}$.Some of these situation can be illustrated by the nucleation of a free stream nucleus as it travels along the streamline containing xi^* as in Figure (2.4)

- $\sigma > -C_{p(xi^*)}$the pressure along the entire trajectory is greater than P_v.
- $\sigma = -C_{p(xi^*)}$ the nucleus encounters $p = p_v$ only for an infinitesimal moment.
- $\sigma < -C_{p(xi^*)}$the nucleus experiences $p < p_v$ for a finite time [3] [8].

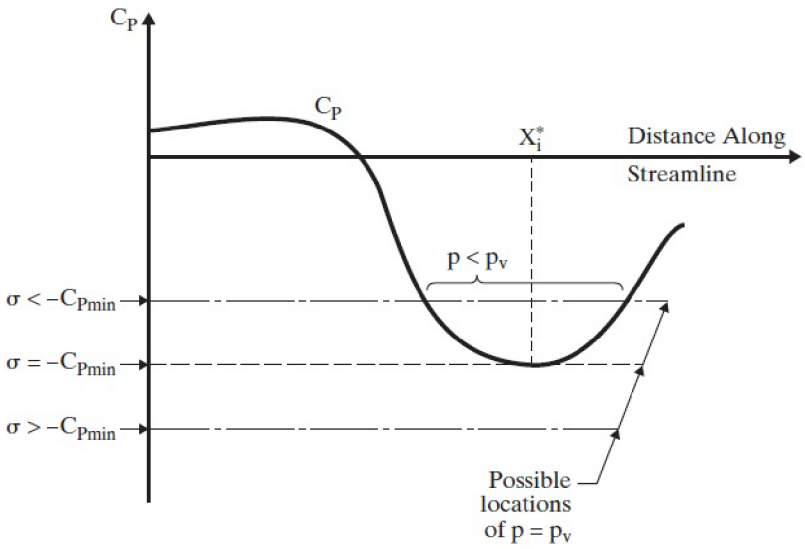

Figure 2-5 Schematic Pressure distribution on a streamline

2.6 Bubble Growth

As above we considered as the initial formation of bubble, nucleation, now we discuss the dynamic of the bubble. To make a simple case, a spherically symmetric single bubble in an infinite domain of liquid at rest with a uniform temperature is considered. The concept of ***Rayleigh-Plesset Equation***, a spherical bubble of radius, R(t) in time t, in an infinite domain of liquid at temperature T_∞ and pressure $P_\infty(t)$ respectively far from the bubble. Temperature gradient is eliminated since the uniform temperature, T_∞ is considered. P_∞ is the control pressure that will drive the bubble dynamic. Figure (2.6) shows, the radius of the bubble at time R(t), radial outward position to *r* in infinite liquid which distance from the center of the bubble with designated the radial outward velocity *u(r,t)*, pressure *p(r,t)* and temperature *T(r,t)*.

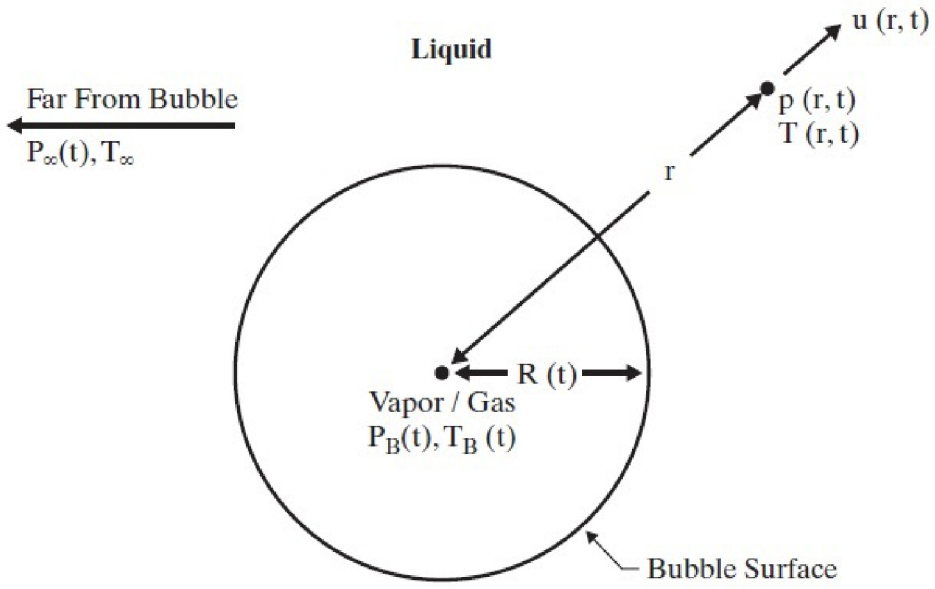

Figure 2-6 Schematic of spherical bubble growth in an infinite liquid

With gas content in bubble Rayleigh- Plesset equation can be express as

$$R\ddot{R} + \frac{3}{2}(\dot{R})^2 + \frac{4\nu_L}{R}\dot{R} + \frac{2S}{\rho_L R} = \frac{P_{B(t)} - P_{\infty(t)}}{\rho_L} + \frac{P_{g0}\left(\frac{R_O}{R}\right)^{3k}}{\rho_L} \qquad (2.8)$$

Where R_o is the initial bubble radius, R is the bubble radius at time t, $\dot{R}$ and $\ddot{R}$ are first and second order of derivatives with respect to time. ν_L is kinematic viscosity, S is the surface tension,k is the gas constant. [9;3].

By integrating equation (2.8) assume with an inviscid case at applied pressure $P_\infty^* < P_{\infty(0)}$ asymptotic bubble growth rate $R \gg R_0$ can get:

$$\dot{R} \cong \sqrt{\frac{2}{3}\frac{P_B - P_\infty^*}{\rho_L}} \qquad (2.9)$$

2.7 Bubble Collapse

A bubble will shrink after some time of growth according to Rayleigh-Plasset equation, bubble radius will attain its minimum value at some time. By making hypothetical problem, there is no gas content and surface tension, the applied pressure is $P_B < P_\infty^*$, bubble decrease rate is

$$\dot{R} \cong -\sqrt{\frac{2}{3}\frac{P_\infty^* - P_B}{\rho_L} - \left(\frac{R_0}{R}\right)^3 - 1} \qquad (2.10)$$

When bubble radius goes to zero and at that time have an infinite inward velocity, by numerical integration by Rayleigh (1917) to obtain τ, time required to collapse from $R = R_0$ to $R = 0$. When bubble fully disappear [3]:

$$\tau \cong 0.915 R_0 \sqrt{\frac{\rho_L}{P_\infty^* - P_B}} \qquad (2.11)$$

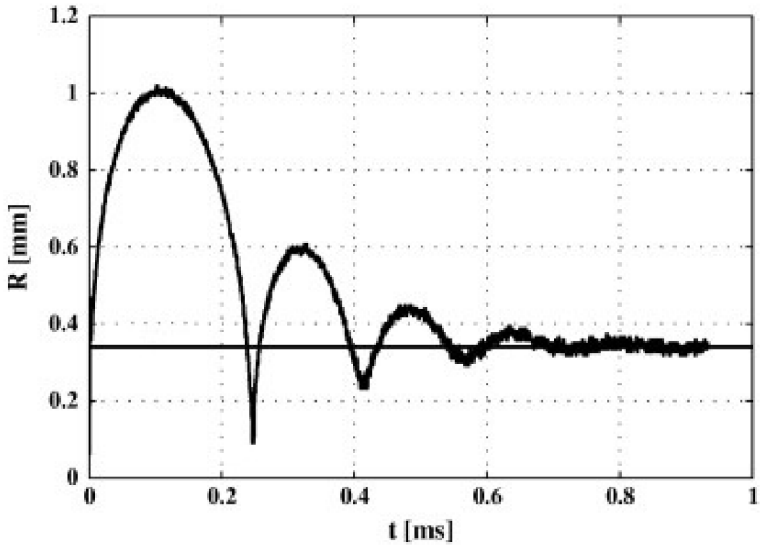

Figure 2-7 Typical bubble radius-time curve[10]

2.8 Bubble Shape Distortion during bubble collapse

Spherical bubble shape can be influenced by gravity, pressure gradients and non-uniform pressure turbulence flow. Plesset and Chapman calculated the deformation of the bubble interface evolution for various distances from the wall and free surface. Surface tension, viscosity and compressibility of liquid are negligible and there is no gas content. The velocity potential φ can be calculated from the Laplace equation $\Delta\varphi = 0$ at a given instant time t. The velocity on the interface can be deduced from the velocity potential. The potential velocity at given instant time at the bubble surface is by generalized Bernoulli equation;

$$\left.\frac{d\varphi}{dt}\right|_{interface} = \frac{\partial\varphi}{\partial t} + \vec{V}.\overrightarrow{grad}\varphi = \frac{P_\infty - P_v}{\rho} + \frac{V^2}{2} \qquad (2.12)$$

2.8.1 Bubble collapse close to a wall

During the collapse close to the solid wall bubble is subjected to the pressure gradient in the direction normal to the surface. This gradient is caused by the higher flow velocity in the gap between the bubble and the wall. The lower pressure closes to the wall move the bubble towards the wall. The bubble shape is deformed and the scale of the deformation depends on the distance between the wall and the bubble center which is noted as a proximity parameter can be defined as:

$$\gamma = \frac{H}{R_{max}} \qquad (2.13)$$

where h is the distance between the bubble center and the wall the R_{max} is maximum bubble radius. Note that the jet produced by the bubble towards the wall is detected by the PVDF sensor.

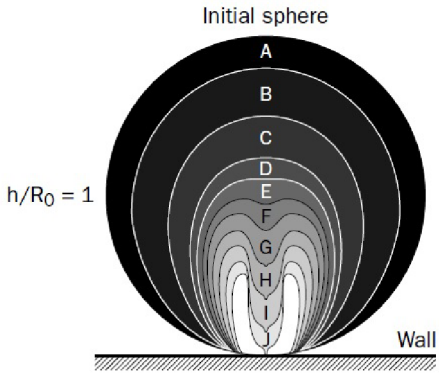

Figure 2-8 distortion shape of a bubble collapse close to the wall

2.9 Microjet & Shockwave

Bubble collapses are accompanied by microjet of a high velocity and strong emission of shockwave or acoustic wave which produce cavitation noise and erosion. Microjet velocity, V_j, normal to the wall can be estimated using the water-hammer formula of Joukowski and Allievi

$$\Delta p = \rho c V_j \quad (2.14)$$

where c is the sound velocity in a liquid medium. From this equation, the velocity of the microjet can be roughly estimated.

Considering for water pressure impact of $\Delta p = 150MPa$, the bubble diameter of 1mm, microjet diameter about 0.1mm, and the sound velocity of water is 1500m/s which gives 0.03μs duration of the pressure pulse. The duration value is will be increased with the bubble size. The duration of the microjet pressure pulse can be calculated by the following equation [1].

$$\tau = \frac{d}{2c} \quad (2.15)$$

where c is the sound velocity of the liquid medium, d is microjet diameter, τ is the microjet pressure pulse duration.

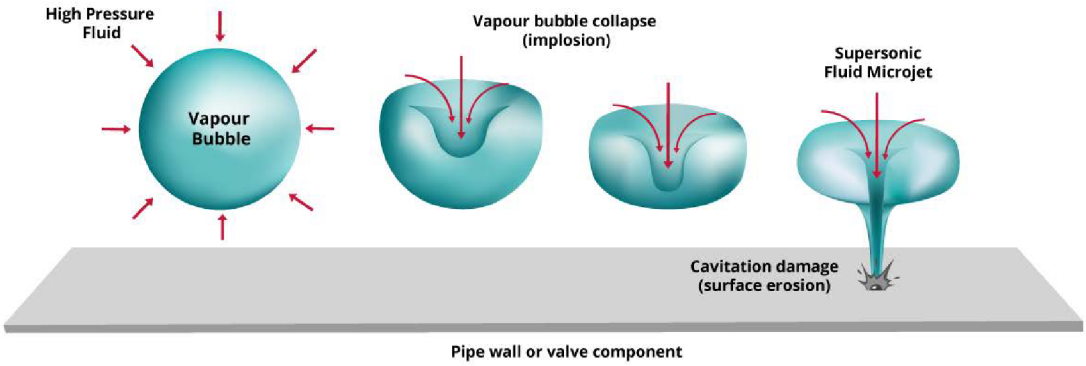

Figure 2-9 Formation of a microjet

3. A REVIEW OF METHODS USED FOR THE CALIBRATION OF PIEZOELECTRIC FILM SENSORS

3.1 Piezoelectric working principle

The piezoelectric effect was first discovered by the brothers Pierre Curie and Jacques Curie in 1880. The name Piezo came from an ancient Greek word *piezein* means press or squeeze. The piezoelectric effect is linear electromechanical interaction when mechanical force subjected to the crystalline materials becomes electrically polarized with no inversion symmetry. The electric voltage generated by tension and compression is directly proportional to the applied force. Figure-3.1(a) shows a typical composition of an electrode where, a layer of free charge was attached at the surface electrode. When external force is applied in the direction perpendicular to the crystal surface distance between the positive and negative electrode decreases. This result in the decrease of t the electric polarization strength and release the free charge, shown in Figure- 3.1(b). Similarly, when the external force causes the increase the distance between the positive and negative

electrode. The electric polarization strength increases and the surface electrodes absorb free charge from the outside as in Figure-3.1(c) [11].

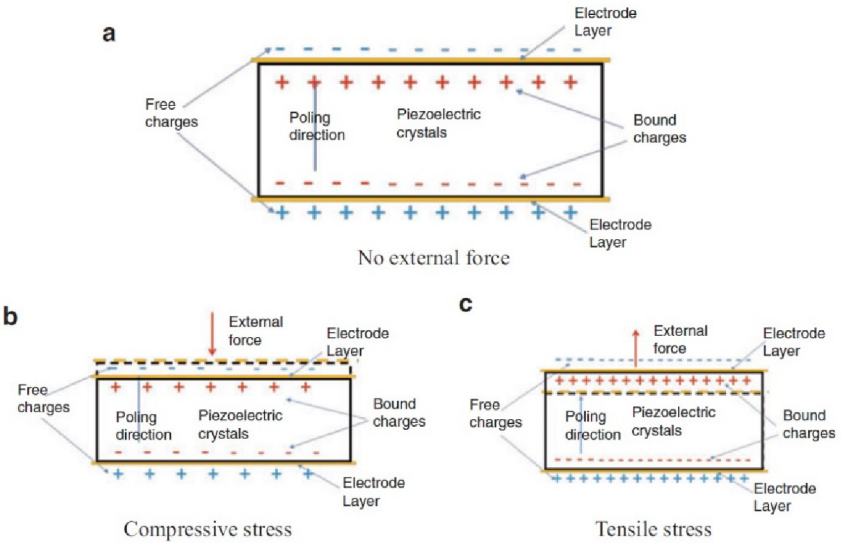

Figure 3-1 Schematic of the energy conversion with piezoelectric effect | (a) no external force (b) Compressive stress (c) Tensile stress

3.1.1 Piezoelectric polyvinylidene fluoride (PVDF)

Polyvinylidene fluoride comprises of a long-chain polymer of many identical repeat units also known as monomer structure. Each unit of the molecule is a CF_2CH_2. These molecules are highly polar due to positively charged hydrogen atoms and negatively charged fluoride atoms, as shown in Figure (3-2). These elementary units are linked chemically to create a chain in the polymerization process. The PVDF molecular weight is about 100 kg/mol corresponding to around 2,000 monomers extended length of 0.5µm [12].

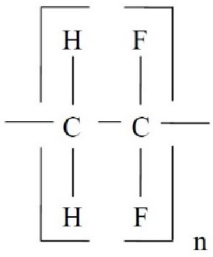

Figure 3-2 Polyvinylidene fluoride molecule

Piezoelectric properties in PVDF were discovered by Kawai in 1969 by subjecting the polymer to the mechanical stretching and electrical field. PVDF has five crystalline phases identified as α, β, γ, δ and ε. In the *α*-Phase opposing directions, a nearly non-polar structure resulting in partial dipole cancellation. The polar crystal structure β, γ, δ are electroactive properties, the dipole is parallel assured non-zero dipole moment. In β-phase all dipole moments point in the same direction which response piezoelectric is the highest. γ and δ phases are slightly polar but their piezoelectric properties are much lower than β-phase.

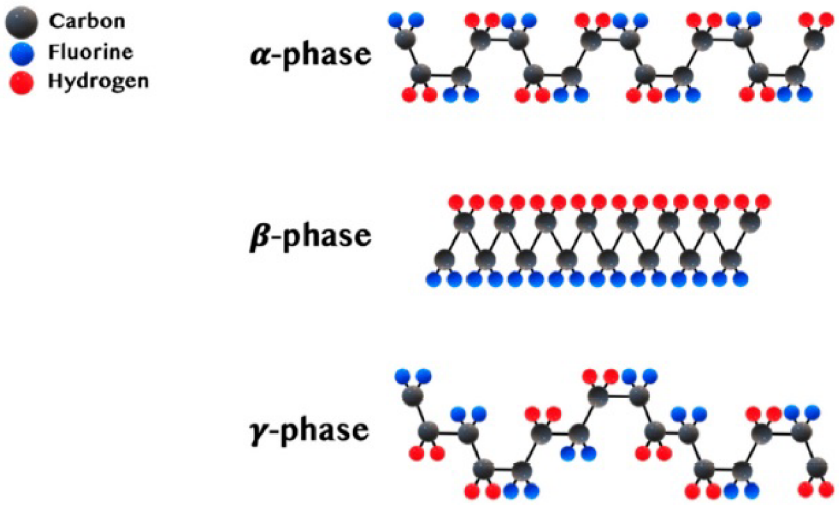

Figure 3-3 3 Main phases of Polyvinylidene fluoride (PVDF)

3.1.2 Piezoelectric General equations

The constitutive relations describing the behaviors of piezoelectric materials can be derived from the thermodynamic principle. A tensor notation is normally used to identify the coupling between mechanical and electrical coefficients. The label the axis directions as "1" and "2" are the stretch direction in the plane of the film. The polarization axis (perpendicular to the surface of the film) is noted as "3". Additionally, shear planes are indicated by subscripts "4", "5", "6" are noted perpendicular to directions "1", "2", "3" respectively as shown in Figure 3-4. [12]

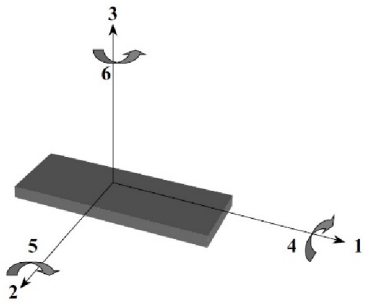

Figure 3-4 Tensor directions for defining the constitutive relations

There can be described four constants in piezoelectricity d_{ij} $e_{ij,}$ h_{ij} g_{ij} by equations in following (Table 3.1). These constants are related to dielectric variable (electric displacement D and electric field E) and elastic coefficients (Strain S and mechanical Stress T).

Equations	Meaning	SI Units
$d_{ij} = (dD_i/dT_j)^E = (dS_j/dE_i)^T$	piezoelectric coefficients for strain-charge form	C/N or m/V
$e_{ij} = (dD_i/dS_j)^E = -(dT_j/dE_i)^S$	piezoelectric coefficients for stress-charge form	C/m or N/Vm
$h_{ij} = (dE_i/dS_j)^D = -(dX_j/dD_i)^S$	piezoelectric coefficients for stress-voltage form	V/m or N/C
$g_{ij} = (dD_i/dT_j)^D = (dS_j/dD_i)^T$	piezoelectric coefficients for strain-voltage form	Vm/N or m^2/C

Table 3-1 Definitions for Piezoelectric constant

In Table3-1, the first two equations correspond to the direct piezoelectric effect. While the last two equations refer to the inverse piezoelectric effect. The superscripts of "E" denotes zero electrified in closed circuit, "D" is zero electric induction in (open circuit), "T" indicates zero mechanical stress when a free sample and S correspond zero strain in fixed sample. The subscripts i and j are 1-3 and 1-6. The above piezoelectric constants are related to each other by the following constant equations in which "c" is the elastic constant and "ε" is the dielectric constant.

$$c = \frac{e}{d} = \frac{h}{g} \qquad (3.1)$$

$$\varepsilon\varepsilon_0 = \frac{d}{g} = \frac{e}{h} \qquad (3.2)$$

Where ε_0 is the constant permittivity of vacuum, 8.854×10^{-12} (F/m) [13].

3.1.3 Piezoelectric linear constitutive relationship

The linear constitutive piezoelectric equations can be defined using Stress (T), Strain (S), electric displacement (D) and electric field (E) by the following equations.

$$S_j = s_{ji}^E . T_i + d_{jm} . E_m \qquad (3.3)$$

$$D_m = d_{mj} . T_j + \varepsilon_{km}^E . E_k \qquad (3.4)$$

Table 3-2 show a list of symbols used in the following constitutive equations of linear behavior of piezoelectric PVDF materials.

Symbol	Meaning	SI unit
S	Strain	
s	Elastic compliance	m^2/N
T	Stress	N/m^2
d	piezoelectric strain charge constant	C/N or m/V
E	Electric field	V/m
D	Electric displacement	C/m^2
ε	dielectric constant	F/m

Table 3-2 Symbols list of linear piezoelectric equations relations

They can be written as matrix form, the subscripts m and k are 1-3, i and j are 1-6. Where d_{mj} defines electric displacement per unit stress at the constant electric field (C/N) and d_{jm} (m/V) strain per unit field at constant stress.

$$\begin{bmatrix} S_1 \\ S_2 \\ S_3 \\ S_4 \\ S_5 \\ S_6 \end{bmatrix} = \begin{bmatrix} S_{11}^E & S_{12}^E & S_{13}^E & S_{14}^E & S_{15}^E & S_{16}^E \\ S_{21}^E & S_{22}^E & S_{23}^E & S_{24}^E & S_{25}^E & S_{26}^E \\ S_{31}^E & S_{32}^E & S_{33}^E & S_{34}^E & S_{35}^E & S_{36}^E \\ S_{41}^E & S_{42}^E & S_{43}^E & S_{44}^E & S_{45}^E & S_{46}^E \\ S_{51}^E & S_{52}^E & S_{53}^E & S_{54}^E & S_{55}^E & S_{56}^E \\ S_{61}^E & S_{62}^E & S_{63}^E & S_{64}^E & S_{65}^E & S_{66}^E \end{bmatrix} \begin{bmatrix} T_1 \\ T_2 \\ T_3 \\ T_4 \\ T_5 \\ T_6 \end{bmatrix} + \begin{bmatrix} d_{11} & d_{12} & d_{13} \\ d_{21} & d_{22} & d_{23} \\ d_{31} & d_{32} & d_{33} \\ d_{41} & d_{42} & d_{43} \\ d_{51} & d_{52} & d_{53} \\ d_{61} & d_{62} & d_{63} \end{bmatrix} \begin{bmatrix} E_1 \\ E_2 \\ E_3 \end{bmatrix}$$

$$\begin{bmatrix} D_1 \\ D_2 \\ D_3 \end{bmatrix} = \begin{bmatrix} d_{11} & d_{12} & d_{13} & d_{14} & d_{15} & d_{16} \\ d_{21} & d_{22} & d_{23} & d_{24} & d_{25} & d_{26} \\ d_{31} & d_{32} & d_{33} & d_{34} & d_{35} & d_{36} \end{bmatrix} \begin{bmatrix} T_1 \\ T_2 \\ T_3 \\ T_4 \\ T_5 \\ T_6 \end{bmatrix} + \begin{bmatrix} \varepsilon_{11}^E & \varepsilon_{12}^E & \varepsilon_{13}^E \\ \varepsilon_{21}^E & \varepsilon_{22}^E & \varepsilon_{23}^E \\ \varepsilon_{31}^E & \varepsilon_{32}^E & \varepsilon_{33}^E \end{bmatrix} \begin{bmatrix} E_1 \\ E_2 \\ E_3 \end{bmatrix}$$

For a thin film, the matrix of the piezoelectric constant d_{jm} can be expressed in terms of axis directions defined in figure 3-4 earlier.

$$d = \begin{bmatrix} 0 & 0 & d_{31} \\ 0 & 0 & d_{32} \\ 0 & 0 & d_{33} \\ 0 & d_{24} & 0 \\ d_{15} & 0 & 0 \\ 0 & 0 & 0 \end{bmatrix}$$

Where each coefficient of the first subscript is the poling direction and the second subscript is the mechanical deformation of stress. The piezoelectricity is limited to few directions with zero coefficient in the remaining axis. The main coefficients of interest are d_{31} d_{32} d_{33} relate the normal strain in the "1" "2" and "3" in along the poling direction. d_{15} and d_{24} are shear strains related to plane 1-3 and plane 2-3 [14].

The magnetic effects are known to be significantly smaller than the electrical effects, possible to neglect full electromagnetic equations in consideration of piezoelectric behavior. There is no external applied electric field, "E" is zero. Therefore, simplifying equation (3.4) mechanical deflection causes the electric charge generation in PVDF piezoelectric equation becomes:

$$D_m = d_{mj}.T_j \qquad (3.5)$$

In matrix form:

$$\begin{bmatrix} D_1 \\ D_2 \\ D_3 \end{bmatrix} = \begin{bmatrix} 0 & 0 & 0 & 0 & d_{15} & d_{16} \\ 0 & 0 & 0 & d_{24} & 0 & 0 \\ d_{31} & d_{32} & d_{33} & 0 & 0 & 0 \end{bmatrix} \begin{bmatrix} T_1 \\ T_2 \\ T_3 \\ T_4 \\ T_5 \\ T_6 \end{bmatrix}$$

Where stress vector defined as in matrix:

$$\begin{bmatrix} T_1 \\ T_2 \\ T_3 \\ T_4 \\ T_5 \\ T_6 \end{bmatrix} = \begin{bmatrix} T_{11} \\ T_{22} \\ T_{33} \\ T_{23} \\ T_{31} \\ T_{12} \end{bmatrix}$$

The "D" electric displacement is related to the charge generated by the following relation:

$$q = \iint \begin{bmatrix} D_1 & D_2 & D_3 \end{bmatrix} \begin{bmatrix} dA_1 \\ dA_2 \\ dA_3 \end{bmatrix} \qquad (3.6)$$

Where dA_1, dA_2 and dA_3 are the electrode area of the components in plane of 2-3,1-3 and 1-2 respectively. It can be seen that the charge collected, q, depends only on the infinitesimal electrode area **dA** normal to the displacement **D**. The voltage generated across the sensor electrodes V_s is related with charge, q and capacitance of the sensor C_s can be shown as

$$V_s = \frac{q}{C_s} \qquad (3.7) \qquad [14][15].$$

3.1.4 Modes of operation of the PVDF sensor

There are two distinct modes, the 31mode and 33mode to measure stress. The poling direction is usually along the thickness 3 direction in piezoelectric film. The first digit in both modes 31 and 33 indicate the direction of the PVDF polarization direction. The second digit refers to the applied stress direction. As shown in Figure (3.5), In 31mode, the applied stress is in the longitudinal direction. In 33 mode, PVDF sensor acts as a pressure sensor, stress is applied in the 3-polarization direction normal to the 1-2 plane.

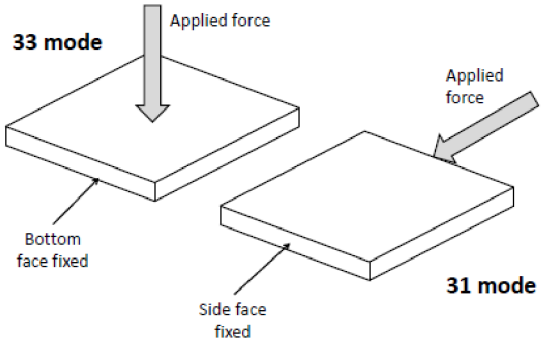

Figure 3-5 PVDF operation mode- 33(left) and 31 (right) [16]

3.2 calibration methods for piezoelectric film sensors

To get to know about flow aggressiveness by cavitation impact, the pitting test cannot give normal stress applied to the flow boundary solid wall but only comparing of yield strength of the material. For the more precise value of flow aggressiveness, a direct measure of normal applied stress by flush-mounted PVDF pressure transducer on flow solid wall. By using the technique of the dislocation of crystal response depends on the direction of the force either

tangential or normal to the surface confirmed that cavitation impact force is chiefly normal to the wall [FILALI et al. 1999b].

There are two main methods of calibration that are commonly used to measure the amplitude and rise time of the applied to the transducer.

Ball drop method which is a steel ball dropped normal direction of transducer. Force can be calculated from the equation of the momentum by measuring the fall and rebound height of the steel ball and the duration of the shock.

Pencil-lead breaking method which is pencil lead is under progressive load up to its rupture. Force on transducer can be calculated by applied weight on apparatus and loading points on the geometry.

3.2.1 Ball drop testing Method

The testing method is using the certain mass of steel-ball, m, which is dropped through the glass tube from the vertical position of a known initial height h_1 on to the PVDF sensor. After hitting to the sensor, rebound height of the ball, second position, h_2 can be obtained by the recording with a camera using slow-motion feature [17]. Deformation of the sensor during the ball impact generates an electric charge which is directly connected to the digital storage oscilloscope device which can get the result as the output voltage. The maximum voltage of U_{max} and duration of the impact time, τ can be determined full width of the maximum voltage as experimentally recorded by a digital oscilloscope.

The obtained maximum voltage from the sensor is converted to force by using the impulse-momentum theorem. The average impact force can be obtained as

$$F_{avg} = \frac{1}{\tau}\int_{t_1}^{t_2} F(t)dt = \frac{m}{\tau}(v_1 + v_2) \qquad (4.1)$$

Where m is the mass of the steel ball, v_1 and v_2 are the velocities of the ball

from the position of a point 1 and 2 respectively. These velocities can be computed by the following equation:

$$v_{1,2} = \sqrt{2gh_{1,2}} \qquad (4.2)$$

where $h_{1,2}$ are the height of the ball from the sensor and g is the gravitational acceleration. The maximum force can be considered as double of the average force which is measured from the shape of the signal [17][18].

$$F_{max} = 2.F_{avg} \qquad (4.3)$$

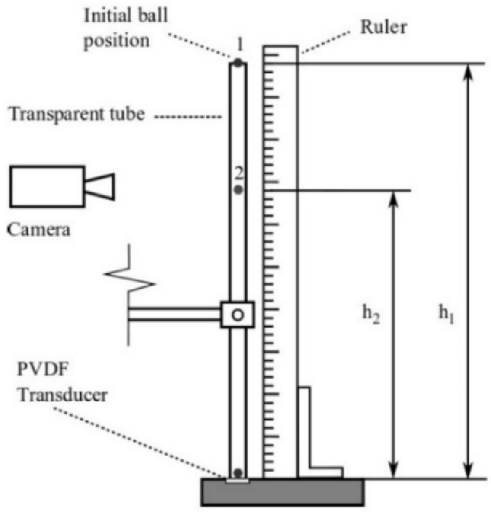

Figure 3-6 Ball drop calibration [Hujer et. al.]

3.2.2 Pencil-lead breaking testing method

The method is based on the release of the static load by breaking the pencil lead which tip place on the PVDF pressure transducer. The described calibration method is adapted from [Soyama et.al]. The assembly consists of a horizontal steel beam. In one side of the beam the pencil lead which place on the transducer and the second side is supported by a knife-edge. In the middle of the horizontal beam block the water bottle is hanged. The weight of the water bottle is slowly increased by pouring water. When a certain amount of water reaches the breaking point of the pencil lead, slowly accumulated static load on the PVDF transducer is suddenly released.

Stopper is installed preventing the beam impact to the transducer. The horizontal beam is shown in Figure (3-7). The weight of the poured water and the weight of the horizontal beam block apparatus and from loading points of the beam geometry for the applied force on the transducer can be calculated[19]. The applied force can be calculated by point load bending moment equation:

$$\sum M_A = 0$$

$$W \times a = B_y \times x \qquad (4.4)$$

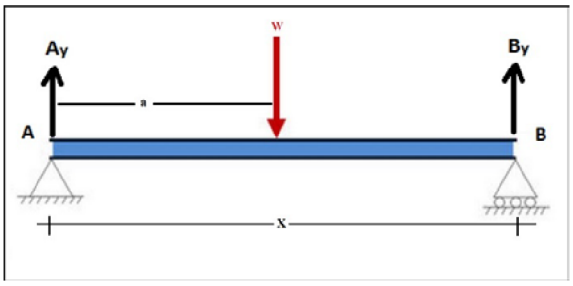

Figure 3-7 Schematic diagram of point load on beam

Where W is the weight of the applied load, a and x are distance. B_y is the reaction load of the beam with acting on the transducer.

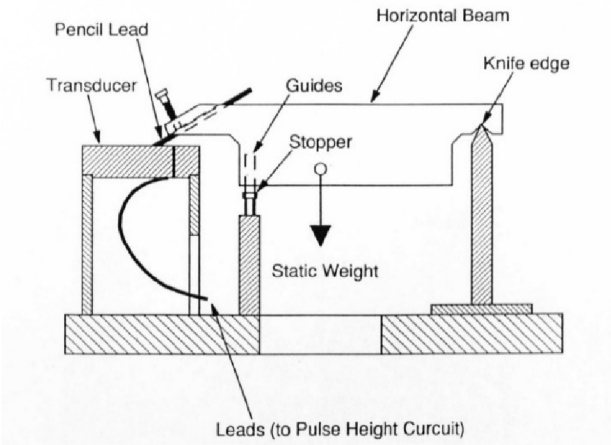

Figure 3-8 Calibration Pencil Lead Breaking Method [Soyama et.al]

4. THE DESIGN OF AN EXPRIMENTAL ASSEMBLY FOR THE REALIZTION THE SELECTED CALIBRATION METHOD

4.1 Sensor

A commercially available PVDF DT series film sensor rectangular elements of Piezo film with silver ink screen printed electrodes which are protected by a thin layer of coating to prevent oxidation on the top layer of silver ink are used. Lead attachment is accomplished using 300 mm rivet lug 28 AWG wire. The DT film transducer can produce more than 10 millivolts per micro strain. The capacitance is directly proportional to the sensitive area and inversely proportional to its thickness. Two types of sensors (DT1-028K/L w/rivets) and (DT1-052K/L w/rivets) are chosen for comparision. [20].

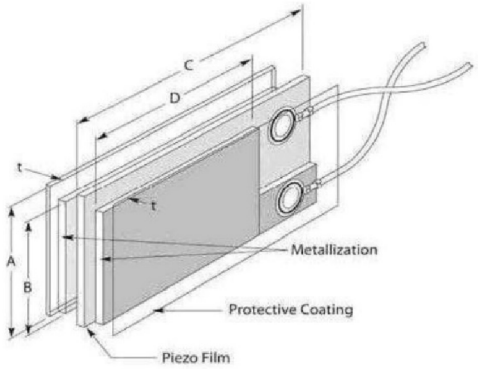

Dimensions in inches (mm)

Model Number	Part Number	Film Thickness	A Film	B Electrode	C Film	D Electrode	Total Thickness (µm)	Cap (nF)
DT1-028K/L w/rivets	1-1002908-0	28 µm	.64 (16)	.484 (12)	1.63 (41)	1.19 (30)	40	1.38
DT1-052K/L w/rivets	2-1002908-0	52 µm	.64 (16)	.484 (12)	1.63 (41)	1.19 (30)	64	.740

Figure 4-1 Dimensions and part numbers of DT series PVDF sensor

The film is mounted on the well-polished metal plate by using cyanoacrylate glue (Loctite Super bond Power flex Gel). The rivet of the sensor is insulted with 15mm electrical tape from the metal platform to avoid the disturbance of electrical signals. The dual wire of the film is welded

to the premium cord BNC cord which is directly connected to the oscilloscope or Data Acquisition System.

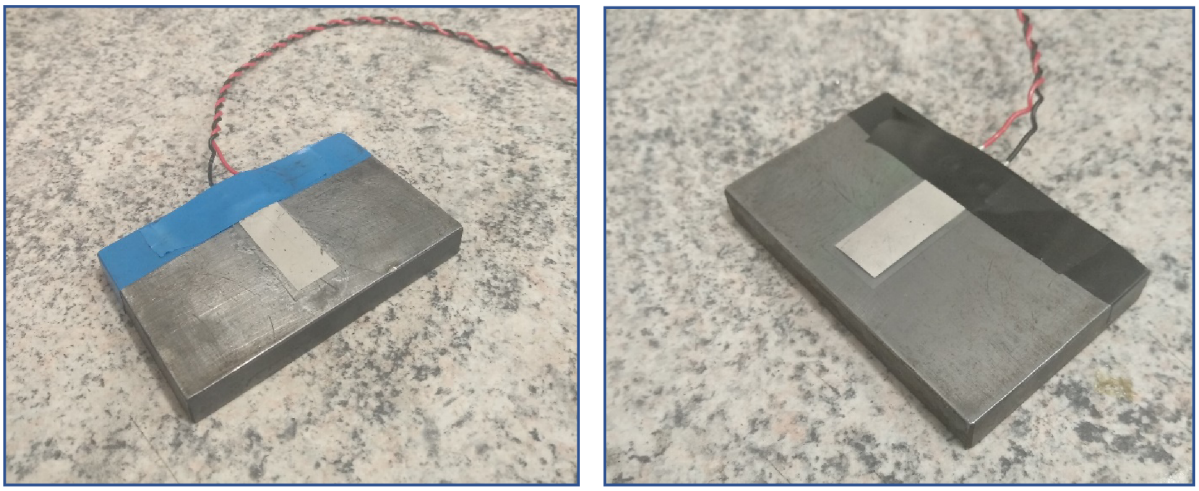

Figure 4-2 MSI PVDF sensors - DT1-028K/L w/rivets (left) & DT1-052K/L w/rivets (right)

4.2 Calibration by the Ball drop Method

In this measurement method, various sizes of steel ball with different weights (0.700g,0.411g, 0.256g and0.0132g 0.263g 0.508g,0.88g, 1.045g and 1.252g) are dropped from a different initial height through a guide tube.(150mm, 300mm, 400mm). In this calibration two different types of PVDF film sensors are used (DT1-028K/L w/rivets) and (DT1-052K/L w/rivets). Each PVDF transducer is mounted on the metal plate by (Loctite Super Bond Flex Gel) cyanoacrylate glue. For preventing the short-circuited by the metal plate and rivet part of the sensor insulated by width 15mm electrical tape. The dual wire lead of the sensor is welded to BNC probe which is connected to the NI PXI-1033 National Instruments Data Acquisition System. The NI PXI-1033 is connected via a PCI card to the laptop. NI Signal Express software is used to analyze the data from the output signal from the measurement devices. The experimental assembly is shown in the figure-(5.3).

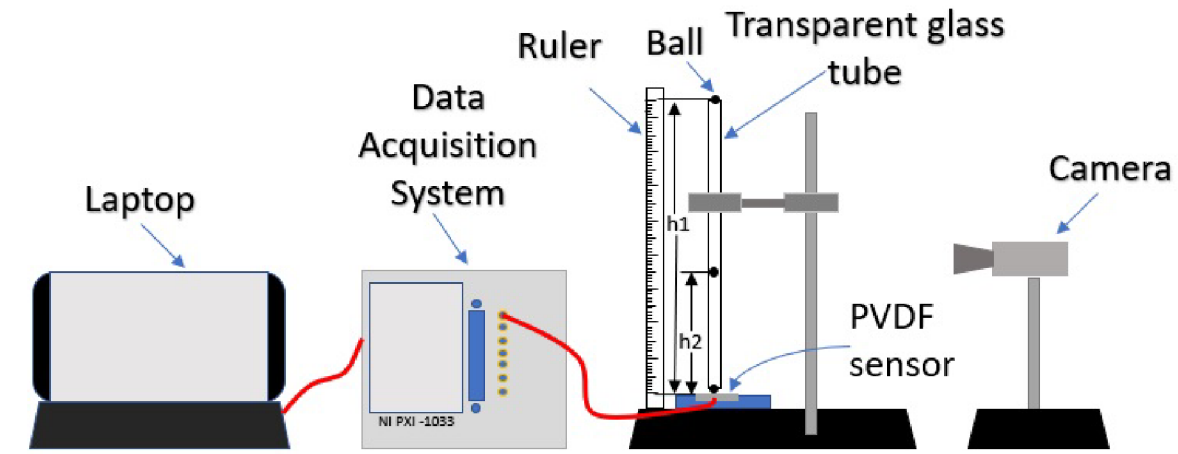

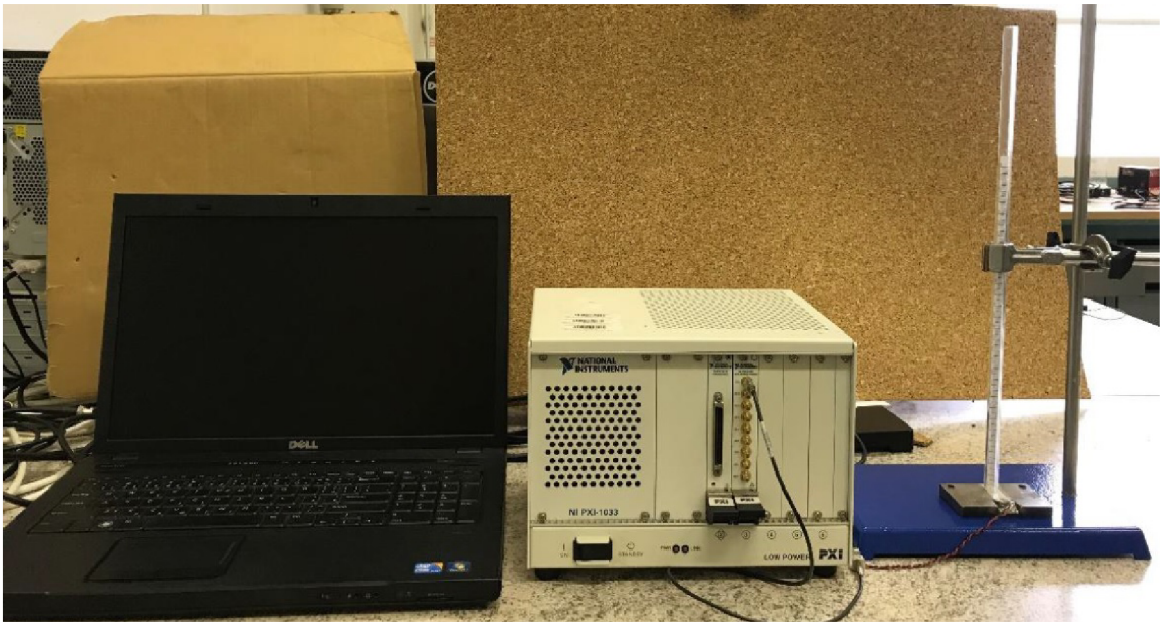

Figure 4-3 Ball Drop method experimental setup

4.2.1 DAQ setting of Ball drop Method

The configuration of the triggering and the signal acquisition NI PXI5105 data acquisition system is as follow:

- Device – NI PXI5105
- Channel – 0

- Probe attenuation – 1:1
- Coupling – DC
- Input Impedance – 1 ohm
- Range – 6V
- Offset – 0V
- Bandwidth – 0 Hz
- Sample Rate – 10 (MS/s)
- Record Length – 20000
- Acquisition – Normal Samples
- Trigger mode – Edge
- Slope – rise time
- Ref position – 0
- Level(V) – 0
- Max Time (s) – 20 s
- Delay (s) – 5m

The data are exported in an Excel format (. xlsx) and picture format (.png or .jpg). There are five calibration tests to perform for each steel ball as shown in figure-(4.4).

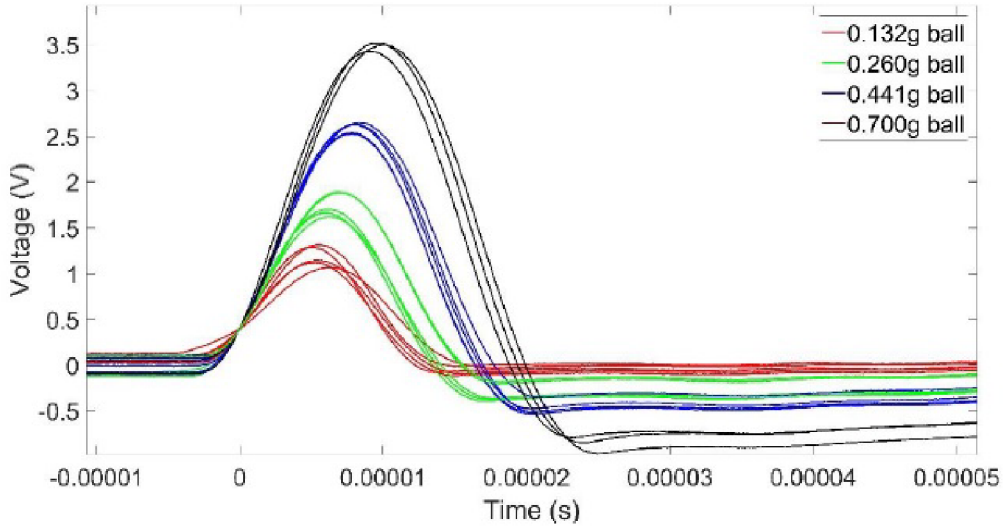

Figure 4-4 initial height 400mm dropped steel balls calibration signal obtained from MSI PVDF- DT1-028K/L w/rivets 400

4.3 Calibration of Pencil-lead breaking Method

A calibration device using a pencil-lead breaking load is developed in order to obtain the calibration value for faster loading. This measurement consists of a steel horizontal beam with a pencil lead at the front end, a knife-edge that has supported at the beam at a rare end and, a hook with a static weight at the center of the beam. The inclined tip of the 2mm pencil lead (KOH-I-NOOR HARDTMUTH), normally used for drawing is located on the pressure transducer PVDF film as shown in figure 4.5. Two types of PVDF sensors were used for the comparison with the ball drop method. The dual wire lead of the sensor is welded to a BNC probe which is connected to the Infinii Vision Oscilloscope (MSO-X-3054A) by Agilent Technologies. The center of the horizontal steel beam with hook is loaded by the plastic bottle with water. The weight is slowly increased by pouring water until the pencil lead breaks. The load at which the pencil breaking point can be changed by types of pencil lead which different hardness and by altering the protruding length of the lead. The load can be measured by the device weight and the amount of water poured into the bottle and geometry of the supporting points and loading point. In this calibration seven calibration tests were performed for each protruding length of the pencil lead.

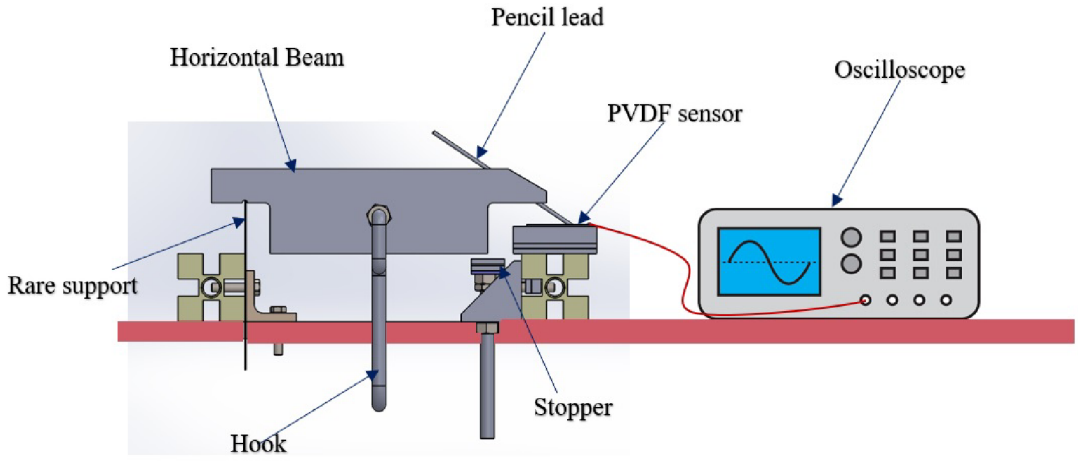

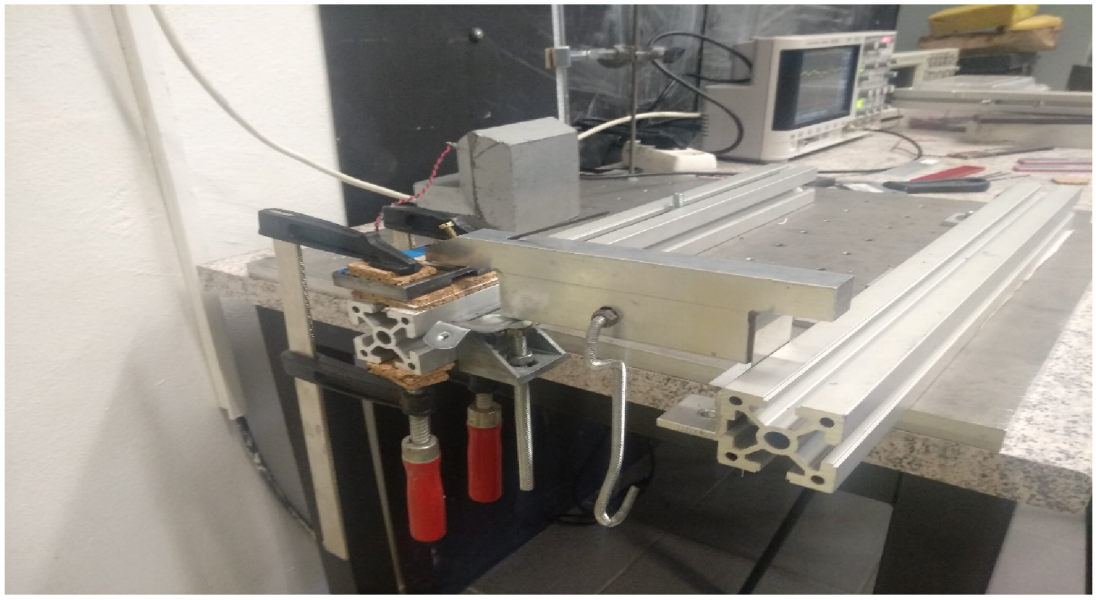

Figure 4-5 Pencil-lead breaking Method Experimental Setup

4.3.1 DAQ setting of Pencil lead Method

The configuration of the triggering and the data acquisition of Infinii Vision Oscilloscope (MSO-X-3054A) by Agilent Technologies listed as follows

- Device – MSO-X-3054A
- Channel – 1
- Probe attenuation – 1:1
- Coupling – DC
- Input Impedance – 1 ohm
- Range – 6V
- Offset – 0V
- Bandwidth – 500 MHz
- Sample Rate – 4 (GS/s)
- Acquisition – Normal Samples
- Trigger mode – Edge
- Slope – fall time

- Ref position – 0
- Level(V) – 0

The data are exported in Excel format (. xlsx) and picture format (.png or .jpg). The figure 4-6 shows typical signal from the pencil lead break calibration.

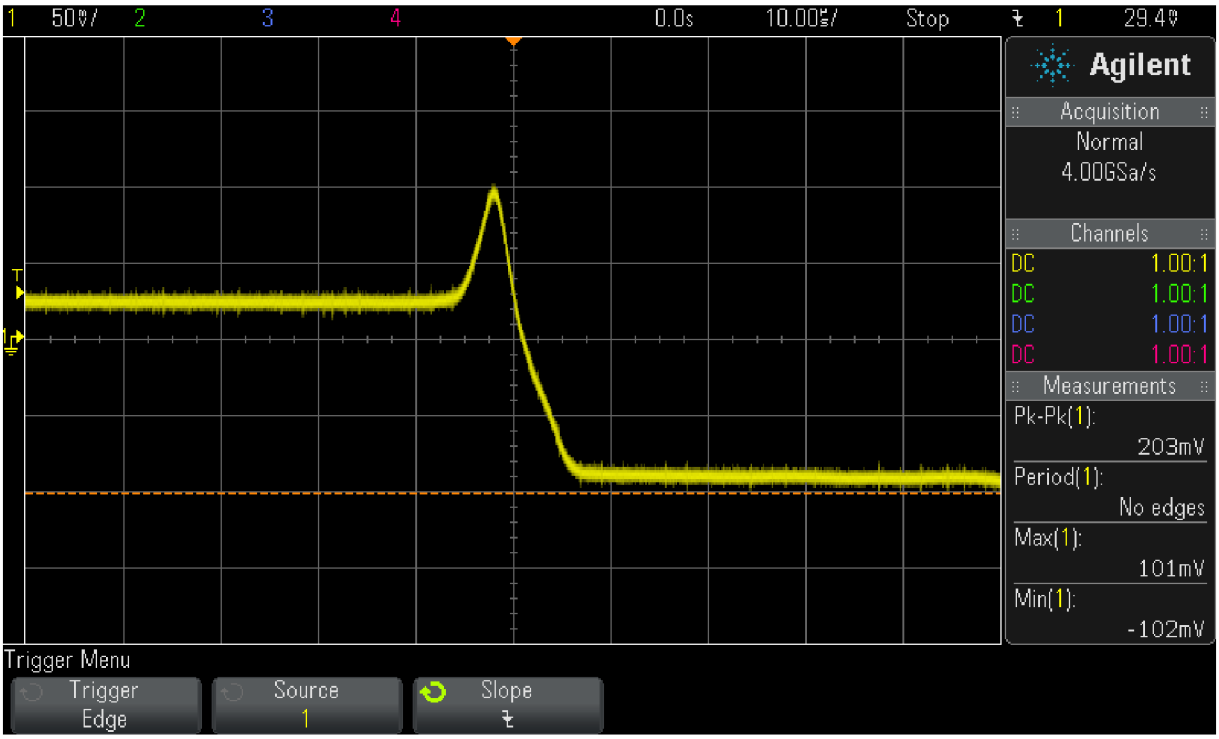

Figure 4-6 2mm diameter H pencil lead 20mm protruding length calibration signal obtained MSO-X-3054A oscilloscope

5. The calibration of piezoelectric film sensors with the selected calibration method

The output signal from the two PVDF sensors, (MSI DT1-028K/L w/rivets) and (DT1-052K/L w/rivets), calibrated with the ball drop and pencil-lead breaking methods is recorded. The experimental results of the maximum output voltage and duration of signal pulse will be analyzed.

5.1 Calibration results of impact force with output voltage

The calibration curve in figure 5-1 is plotted maximum voltage versus four different mass of the steel balls 0.7g, 0.441g, 0.132g and 0.411g are dropped from three different initial heights 150mm,300mm and 400mm from a guide glass tube to the MSI DT1-028K/L w/rivets sensor. It shows linearly increased with the initial height increases.

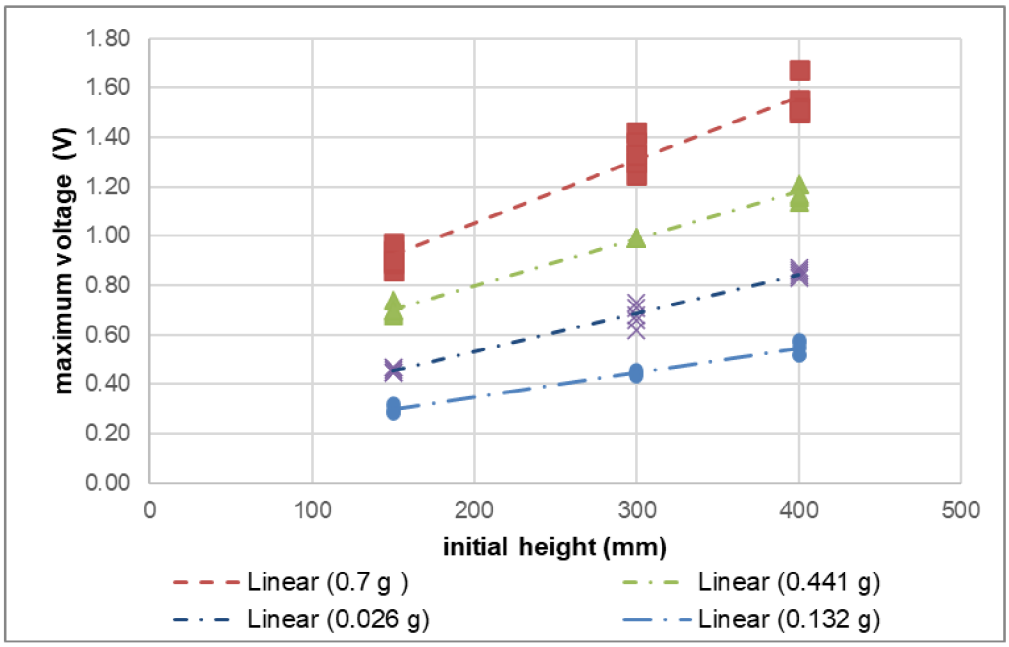

Figure 5-1 MSI DT1-028K/L w/rivets sensor four steel balls dropped from three initial heights

In figure 5-2 and 5-3 were plotted the maximum voltage vs maximum impact load with two different sensors. In figure 5-2 used four different mass of steel balls with three different initial heights dropped into MSI DT1-028K/L w/rivets sensor plotted output voltage per maximum impact force.

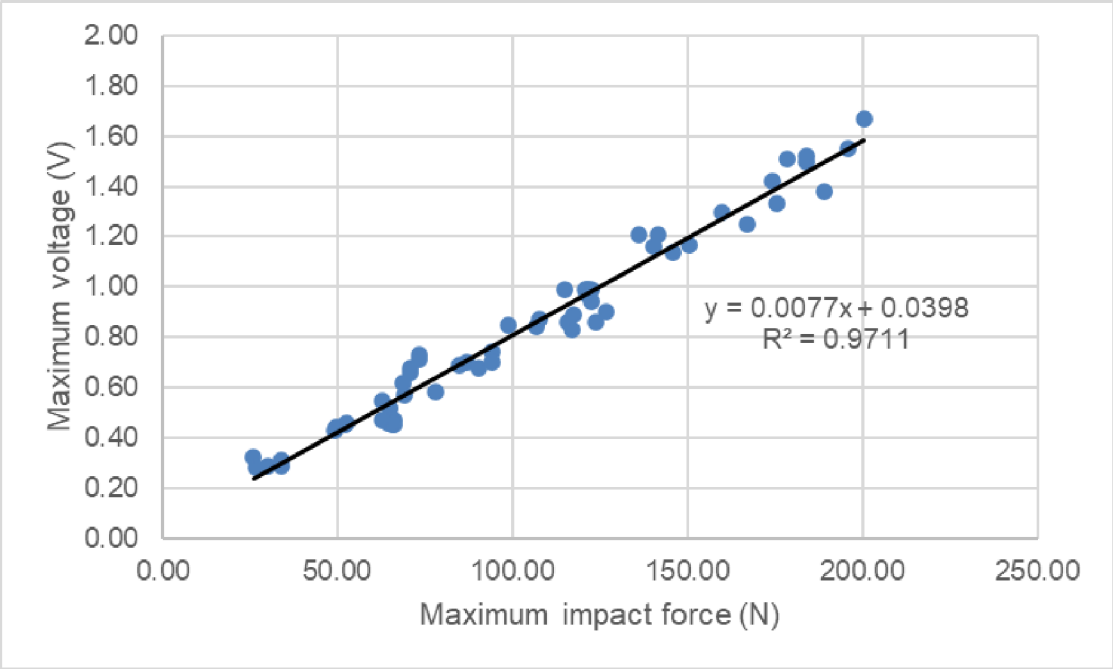

Figure 5-2 MSI DT1-028K/L w/rivets sensor voltage per impact force by drop ball method

In figure 5-3 used four different mass of steel balls dropped from the same initial height 400mm into MSI DT1-052K/L sensor plotted maximum output voltage per maximum impact force.

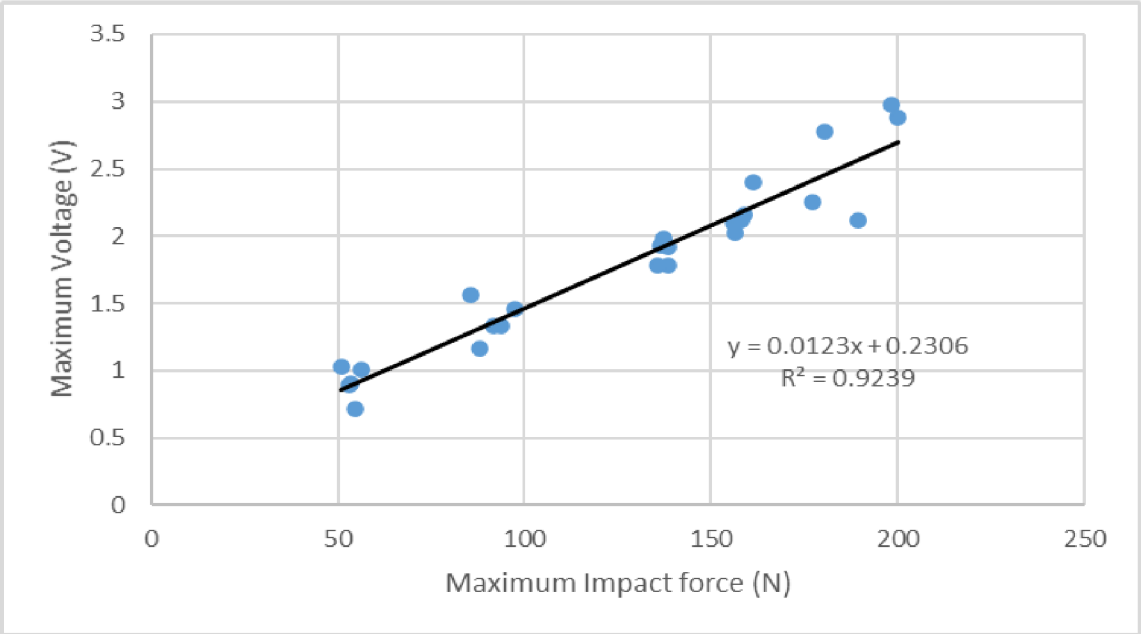

Figure 5-3 MSI DT1-052K/L w/rivets sensor voltage constant per impact force by drop ball method

Figure 5-4 illustrates that DT1-052K/L w/rivets generates a higher voltage than DT1-028K/L when applying the same dynamic impact load.

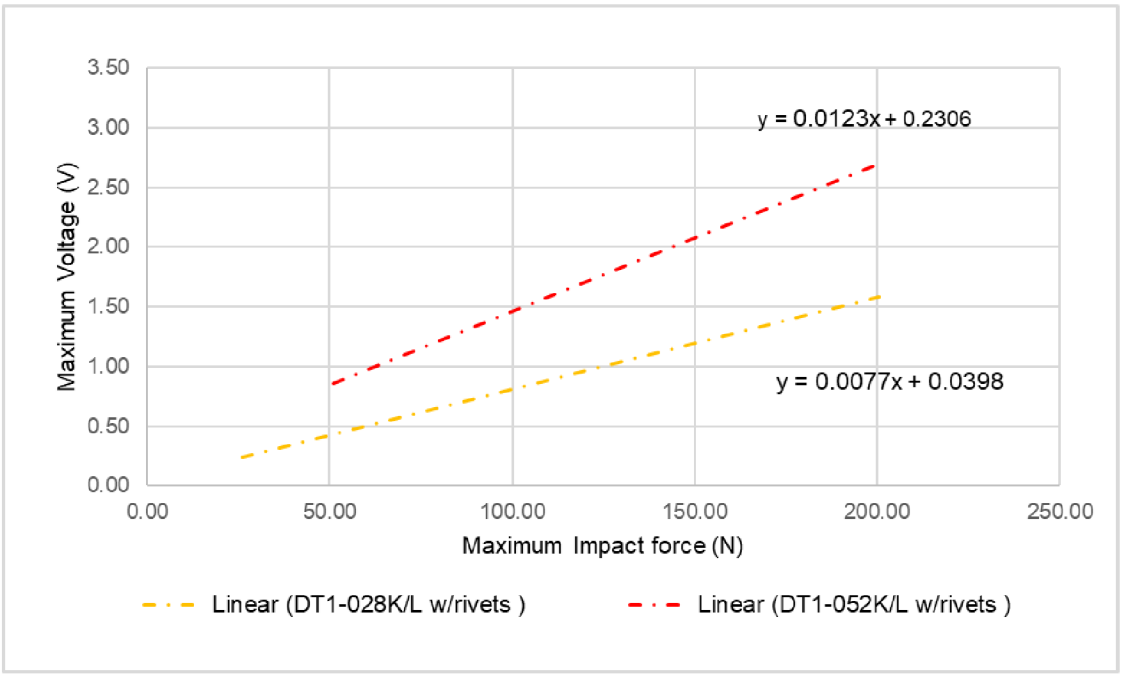

Figure 5-4 PVDF sensors calibration constant

In the following figure5-5 was calibration of pencil lead breaking method with MSI DT1-052K/L sensor same type of H pencil lead with different protruding length 20mm and 15mm. While sensor pencil lead breaking point is too low, maximum release load give out only micro voltage.

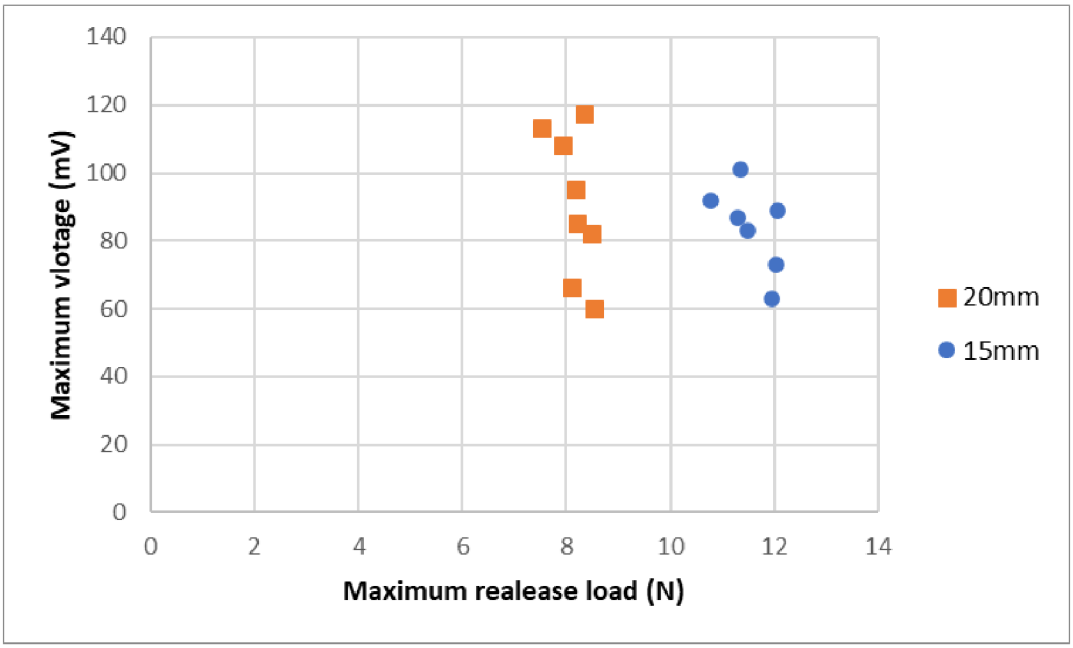

Figure 5-5 MSI DT1-052K/L voltage constant per release load by H pencil lead breaking method

5.2 Calibration results of impact force with duration time

In figure 5-6 is illustrated with four different mass of steel balls are dropped from the three different initial heights into the MSI DT1-028K/L. As shown in figure 5-1, when mass and initial height increase, impact force is larger as a result of larger output voltage generated from the sensor. The following figure5-6 illustrates that larger mass and size results a longer impact duration. The Ball dropped method impact duration is between 20 to 38μs.

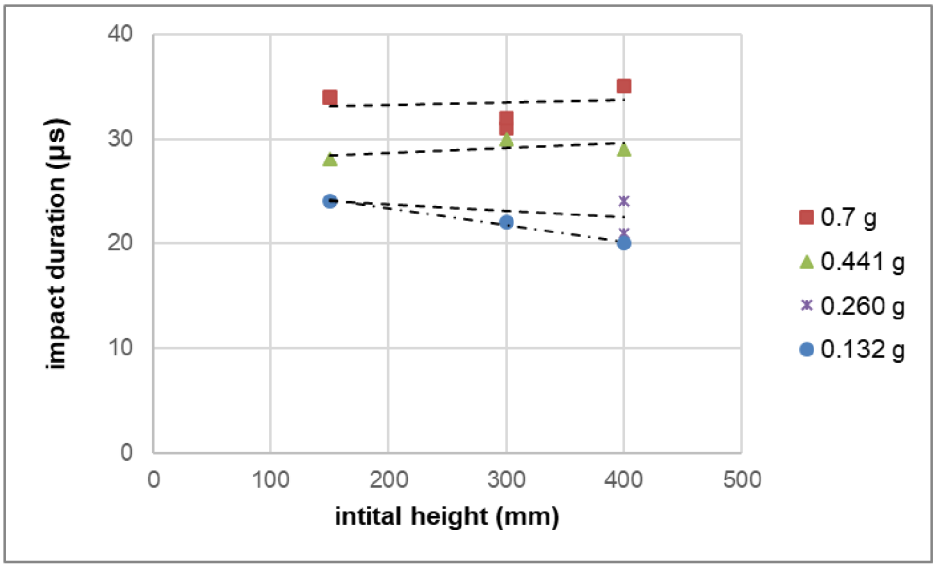

Figure 5-6 impact duration time of four different steel ball dropped from three different initial heights

In figure 5-7 five different mass and size of steel balls dropped from 400mm guided tube into the MSI DT1-052K/L shows the good agreement with Figure 5-6 of impact duration of the ball dropped the method; lager impact force longer impact duration.

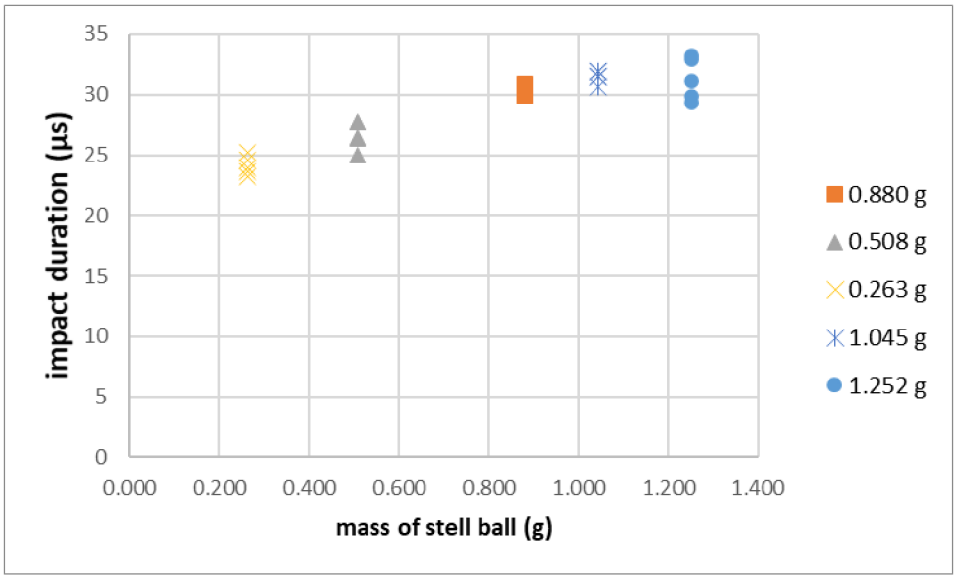

Figure 5-7 impact duration time of five different steel ball dropped from 400mm initial height

In figure 7-8 shows the impact duration of the releasing load on different types of pencil lead and protruding lengths calibration on two different types of sensors. In this result H 15 mm* is calibrated with MSI DT1-028K/L while other tests are with MSI DT1-052K/L sensor. The impact duration time show good agreement duration is around 5 to 11µs.

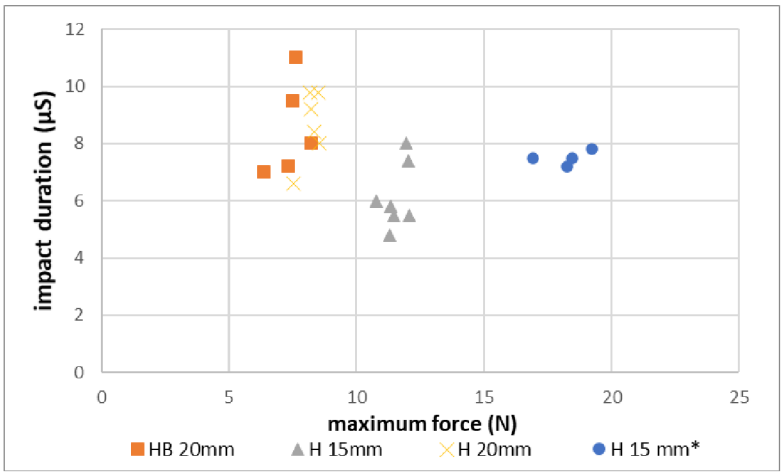

Figure 5-8 impact duration time of releasing load by pencil lead breaking method.

Also show in pencil- lead breaking method, higher releasing load doesn't not affect impact duration time.

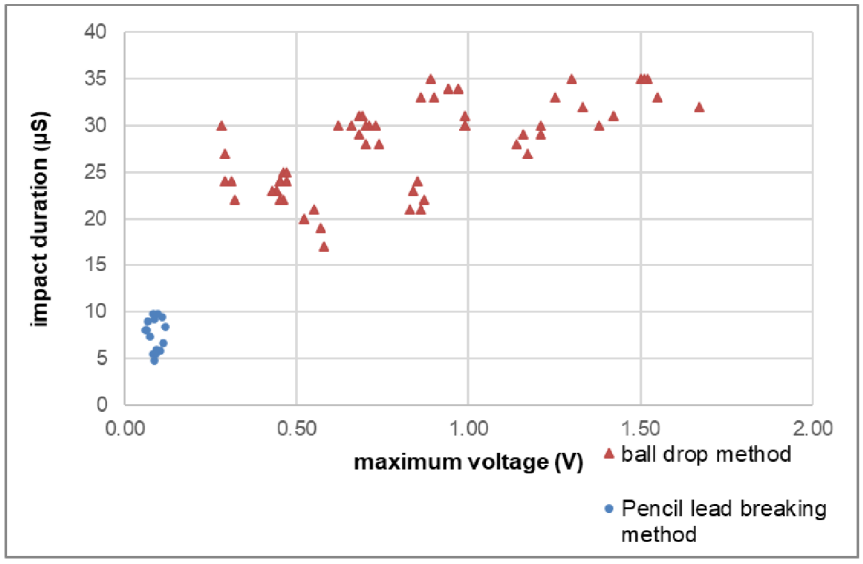

Figure 5-9 comparison of dropping ball and pencil-lead breaking calibration results of impact duration time with maximum voltage signal

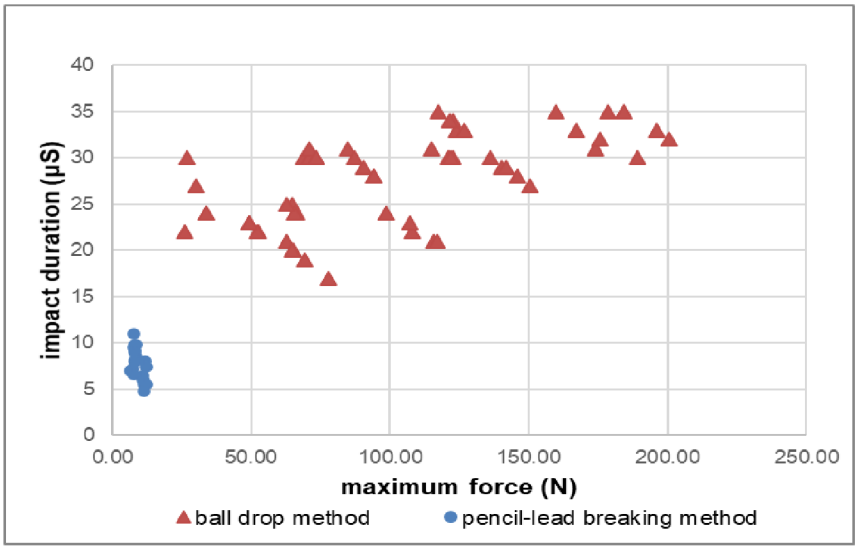

Figure 5-10 comparison of dropping ball and pencil-lead breaking calibration results of impact duration time with maximum loading force

From the above experiments, two calibration methods of the ball-drop and pencil lead breaking results of impact duration time are compared. In figure 5-9 and 5-10 impact duration time versus maximum output voltage from the two sensors and maximum impact or release load. It shows pencil lead breaking method impact duration is three times faster than ball drop methods

6. Recommendation for the application the results obtained by the selected calibration method

It was mentioned before the cavitation erosion is caused be effect accompanying the bubble collapse. The effects most contributing to the erosion are shock wave and bubble jet. As it is known from the literature the duration of the cavitation bubble microjet and shock wave loading is in range from 1 to 5 μs. The standard method used for the calibration of PVDF films is the ball method. This method however gives pulse duration in range between 20 to 40 μs. This can influence the constants obtained from the calibrations.

The pencil lead break method can produce much faster pulse. This method is based on the release of static load after breaking a weak part of the chain. This means that this weak part (the pencil lead in this case) should be capable to break under such a loading which will not destroy the PVDF film itself. The calibration constant obtained by the designed assembly for the pencil lead breaking is applicable only for low forces. The low force corresponds to low voltage and the error of the voltage reading is then higher. For the application of the obtained calibration constants for higher forces it would be necessary to modify the holder for the installation of different types of weak parts (different pencil diameters). It is also seen that the calibration constants obtained by the pencil break calibration method have high deviation. This can be caused by the variation in the quality of the lead.

It can be concluded that with the drop ball calibration technique is easier to obtain higher loading forces, however the pulse duration is higher than form the real cavitation process and also pencil lead break technique. On the other side the pencil lead break calibration technique provides shorter pulses durations but in current state of the experimental setup only small fraction of needed force load.

7. Conclusion

The thesis was focused on the obtaining an appropriate method for the calibration of PVDF sensor for the cavitation aggressiveness measurement. In the first part of the thesis the cavitation fundamentals are introduced as a background of the other parts. A review of appropriate methods for the calibration of piezoelectric film sensors is performed. From the review it is indicated that the pencil lead beak calibration technique gives pulses close to the real cavitation process. For the calibration two experimental setups are designed and assembled. Different types of PVDF sensors are calibrated by the two methods for comparison. The application of the results using the ball drop method to the measurement of the cavitation field is reasonable due to high loadings which can be reached; however, the time duration of the calibration signals differs from the real cavitation process. The application of the calibration constant obtained by the pencil lead break method is possible only for small impact forces. The performed measurements should be extended for the higher loads after the modification of the calibration device.

References

[1]. Jean-Pierre Franc, Jean-Marie Michel. *Fundamentals of Cavitation.* 1. s.l. : Springer Netherlands, 2005. Vol. 76. eBook ISBN 978-1-4020-2233-3.

[2]. Young, F. Ronald. *Cavitation.* Revised ed. edition. s.l. : Imperial College Press, 1999. ISBN 1860941982.

[3]. Brennen, Christopher E. *Cavitation and Bubble Dynamics.* s.l. : Cambridge University Press, 2014. ISBN 1107644763.

[4]. Kompella, Anthony Deku Subramanya. *Cavitation in Engine Cooling Fluid due to Piston-Cylinder Assembly forces.* Karlskrona, Sweden : Blekinge Institute of Technology, 2006. ISRN: BTH-AMT-EX--2006/D-13-SE.

[5]. Yasui, Kyuichi. *Acoustic Cavitation and Bubble Dynamic.* s.l. : Springer International Publishing, 2018. eBook ISBN 978-3-319-68237-2.

[6]. *Bubble Power and Ultrasound.* Ali Alhelfi, Bengt Suden. 11, s.l. : International Journal of Enhanced Research in Science Technology & Engineering, 2013, Vol. 2, pp. 130--134. ISSN 2319-7463.

[7]. *Nucleation.* Wan Nur Athirah Mazli, Mohd Afnan Ahmad and Shafirah Samsuri. 2019. DOI: 10.5772/intechopen.90164.

[8]. *An Introduction to Cavitation Fundamentals.* Brennen, Christopher E. s.l. : WIMRC Forum, 2011.

[9]. Prosperetti, Milton S. Plesset & Andrea. *Bubble Dynamics and Cavitation.* s.l. : Annual Reviews, 1977. ISSN 0066-4189.

[10]. *The effect of high viscosity on compressible and incompressible Rayleigh–Plesset-type bubble models.* Ferenc Hegedűs, Sandra Koch, Walter Garen, Zoltán Pandula, György Paál, László Kullmann, Ulrich Teubner,. Pages 200-208, s.l. : International Journal of Heat and Fluid Flow, 2013, Vol. 42. https://doi.org/10.1016/j.ijheatfluidflow.2013.04.004.

[11]. Deng L., Wen Z., Zhao X. *MEMS Piezoelectric Vibration Energy Harvesters.* s.l. : Springer, Singapore, 2018. ISBN 978-981-10-2798-7.

[12]. Broadhurst M.G., Davis G.T. *Piezo- and pyroelectric properties.* [ed.] Sessler G.M. Berlin, Heidelberg : Springer, 1980. Vol. 33. ISBN 978-3-540-70750-9.

[13]. Ounaies, J. S. Harrison Z. Piezoelectric Polymers. [book auth.] Herman Francis Mark. *Encyclopedia of Polymer Science and Technology.* Hampton, Virginia : NASA Langley Research Center, 2001.

[14]. *Fundamental Understanding of Piezoelectric Strain Sensors.* Chopra, Jayant Sirohi and Inderjit. 246, s.l. : Journal of Intelligent Material Systems and Structures, 2000, Vol. 11. DOI: 10.1106/8BFB-GC8P-XQ47-YCQ0.

[15]. MIKA, BARTOSZ. *DESIGN AND TESTING OF PIEZOELECTRIC SENSORS.* s.l. : Texas A&M University, Texas A&M University.

[16]. *Detection of in-plane stress waves with Polyvinylidene.* Kotian, Kunal. s.l. : The Ohio State University, 2013.

[17]. *Calibration of PVDF Film Transducers for the Cavitation Impact Measurement.* Jan Hujer, Miloš Müller. Liberec : EPJ Web of Conferences, 2017G. https://doi.org/10.1051/epjconf/201818002036.

[18]. *Photolithographically Home-Made PVDF Sensor for Cavitation Impact Load Measurement.* Jan Hujer, Millos Muller, Tomas Korinek,Petra Dancova. s.l. : MATEC Web of Conferences, 2020. DOI: 10.1051/matecconf/202032801004.

[19]. *A New Calibration Method for Dynamically Loaded Transducers and its Application to Cavitation Impact Measurement.* Htoshi Soyama, Andrzej Lichtarowicz, Takahiro Momma, Edward J. Williams. 712-718, s.l. : Jorunal of Fluids Engineering, 1998, Vol. 120(4). https://doi.org/10.1115/1.2820728.

[20]. connectivity, TE. *DT SERIES ELEMENTS WITH.* s.l. : Measurement Specialties, Inc. https://www.te.com/commerce/DocumentDelivery/DDEController?Action=showdoc&DocId=Data+Sheet%7FDT_Series_with_Riveted_Leads%7FA1%7Fpdf%7FEnglish%7FENG_DS_DT_Series_with_Riveted_Leads_A1.pdf%7FCAT-PFS0005.

Appendix

A. 1 ball drop method Calibration data of the MSI DT1-028K/L w/rivets PVDF sensor

Trail	Mass of ball (g)	h1 (mm)	h2 (mm)	V1 (m/s)	V2 (m/s)	t_1 (µs)	t_2 (µs)	t (µs)	U max (V)	F max (N)
1.1	0.700	400	168	2.80	1.82	995	1028	33	1.55	195.87
1.2	0.700	400	166	2.80	1.80	994	1029	35	1.50	184.24
1.3	0.700	400	165	2.80	1.80	995	1030	35	1.52	184.03
1.4	0.700	400	140	2.80	1.66	994	1029	35	1.51	178.35
1.5	0.700	400	162	2.80	1.78	995	1027	32	1.67	200.56
2.1	0.441	400	170	2.80	1.83	995	1025	30	1.21	136.06
2.2	0.441	400	171	2.80	1.83	994	1022	28	1.14	145.94
2.3	0.441	400	167	2.80	1.81	994	1023	29	1.16	140.25
2.4	0.441	400	176	2.80	1.86	994	1023	29	1.21	141.72
2.5	0.441	400	166	2.80	1.80	996	1023	27	1.17	150.47
3.1	0.260	400	178	2.80	1.87	995	1016	21	0.86	115.64
3.2	0.260	400	189	2.80	1.93	996	1017	21	0.83	117.05
3.3	0.260	400	158	2.80	1.76	996	1018	22	0.87	107.83
3.4	0.260	400	156	2.80	1.75	993	1017	24	0.85	98.60
3.5	0.260	400	190	2.80	1.93	995	1018	23	0.84	106.99
4.1	0.132	400	250	2.80	2.21	998	1015	17	0.58	77.90
4.2	0.132	400	242	2.80	2.18	998	1017	19	0.57	69.20
4.3	0.132	400	245	2.80	2.19	993	1014	21	0.55	62.78
4.4	0.132	400	230	2.80	2.12	994	1014	20	0.52	65.02
4.5	0.132	400	228	2.80	2.12	993	1013	20	0.52	64.90
5.1	0.700	300	104	2.43	1.43	994	1025	31	1.42	174.08
5.2	0.700	300	117	2.43	1.52	994	1027	33	1.25	167.20
5.3	0.700	300	125	2.43	1.57	993	1028	35	1.30	159.69
5.4	0.700	300	135	2.43	1.63	995	1025	30	1.38	189.17
5.5	0.700	300	128	2.43	1.58	995	1027	32	1.33	175.47
6.1	0.441	300	132	2.43	1.61	992	1023	31	0.99	114.81
6.2	0.441	300	156	2.43	1.75	993	1023	30	0.99	122.76
6.3	0.441	300	146	2.43	1.69	993	1023	30	0.99	121.09
6.4	0.441	300	145	2.43	1.69	993	1023	30	0.99	120.92
6.5	0.441	300	150	2.43	1.72	993	1023	30	0.99	121.76
7.1	0.260	300	122	2.43	1.55	993	1023	30	0.62	68.87
7.2	0.260	300	139	2.43	1.65	993	1023	30	0.66	70.68
7.3	0.260	300	165	2.43	1.80	993	1023	30	0.73	73.24
7.4	0.260	300	163	2.43	1.79	992	1023	31	0.68	70.69
7.5	0.260	300	168	2.43	1.82	993	1023	30	0.71	73.52
8.1	0.132	300	195	2.43	1.96	992	1014	22	0.46	52.59
8.2	0.132	300	180	2.43	1.88	992	1015	23	0.44	49.42
8.3	0.132	300	180	2.43	1.88	993	1016	23	0.44	49.42

Trail	Mass of ball (g)	h1 (mm)	h2 (mm)	V1 (m/s)	V2 (m/s)	t_1 (µs)	t_2 (µs)	t (µs)	U max (V)	F max (N)
8.4	0.132	300	185	2.43	1.91	996	1018	22	0.45	51.98
8.5	0.132	300	177	2.43	1.86	992	1015	23	0.43	49.24
9.1	0.700	150	74	1.72	1.20	993	1026	33	0.86	123.90
9.2	0.700	150	76	1.72	1.22	993	1028	35	0.89	117.47
9.3	0.700	150	81	1.72	1.26	994	1028	34	0.94	122.55
9.4	0.700	150	77	1.72	1.23	992	1026	34	0.97	121.25
9.5	0.700	150	83	1.72	1.28	992	1025	33	0.90	126.92
10.1	0.441	150	81	1.72	1.26	992	1023	31	0.69	84.68
10.2	0.441	150	79	1.72	1.24	992	1022	30	0.70	87.04
10.3	0.441	150	83	1.72	1.28	994	1022	28	0.74	94.24
10.4	0.441	150	81	1.72	1.26	994	1023	29	0.68	90.52
10.5	0.441	150	82	1.72	1.27	990	1018	28	0.70	93.99
11.1	0.260	150	90	1.72	1.33	998	1022	24	0.47	65.96
11.2	0.260	150	92	1.72	1.34	1000	1024	24	0.45	66.28
11.3	0.260	150	99	1.72	1.39	1000	1025	25	0.46	64.67
11.4	0.260	150	88	1.72	1.31	998	1022	24	0.45	65.64
11.5	0.260	150	87	1.72	1.31	998	1023	25	0.47	62.86
12.1	0.132	150	95	1.72	1.37	994	1018	24	0.29	33.89
12.2	0.132	150	96	1.72	1.37	994	1018	24	0.31	33.97
12.3	0.132	150	95	1.72	1.37	995	1022	27	0.29	30.12
12.4	0.132	150	10	1.72	0.44	997	1019	22	0.32	25.90
12.5	0.132	150	92	1.72	1.34	990	1020	30	0.28	26.92

A.2 ball drop method Calibration data of the MSI DT1-052K/L w/rivets PVDF sensor

Trail	Mass of ball (g)	h1 (mm)	h2 (mm)	V1 (m/s)	V2 (m/s)	t_1 (µs)	t_2 (µs)	t (µs)	U max (V)	F max (N)
1.1	0.880	400	186	2.801428	1.910319	92.67	122.58	29.906	1.92	138.6456847
1.2	0.880	400	198	2.801428	1.970979	90.90	121.20	30.3	1.78	138.6045789
1.3	0.880	400	195	2.801428	1.955991	90.90	121.79	30.8896	1.78	135.5319824
1.4	0.880	400	179	2.801428	1.874028	92.27	122.38	30.113	1.93	136.6320606
1.5	0.880	400	189	2.801428	1.925664	92.67	122.97	30.2998	1.98	137.2893789
2.1	0.508	400	177	2.801428	1.863529	91.88	119.63	27.7418	1.56	85.42337612
2.2	0.508	400	197	2.801428	1.965996	91.10	117.57	26.4718	1.33	91.48797823
2.3	0.508	400	206	2.801428	2.010403	89.33	117.07	27.7416	1.17	88.11352716
2.4	0.508	400	217	2.801428	2.063381	91.29	117.66	26.3651	1.33	93.7346316
2.5	0.508	400	201	2.801428	1.985855	92.67	117.66	24.9878	1.46	97.325089
3.1	0.263	400	221	2.801428	2.082311	94.07	118.05	23.977	0.9	53.56898145
3.2	0.263	400	232	2.801428	2.133504	94.07	118.64	24.567	0.89	52.83051299
3.3	0.263	400	220	2.801428	2.077595	94.05	119.23	25.1846	1.03	50.95109874
3.4	0.263	400	225	2.801428	2.101071	92.47	116.08	23.611	0.72	54.60833223
3.5	0.263	400	235	2.801428	2.147254	95.03	118.25	23.2168	1.01	56.05869183
4.1	1.045	400	200	2.801428	1.980909	95.23	126.71	31.48	2.16	158.7529307
4.2	1.045	400	197	2.801428	1.965996	93.65	125.53	31.8741	2.02	156.3011418
4.3	1.045	400	195	2.801428	1.955991	94.64	126.51	31.8743	2.1	155.9721424
4.4	1.045	400	192	2.801428	1.940886	96.80	127.50	30.693	2.4	161.460879
4.5	1.045	400	196	2.801428	1.961	94.64	126.12	31.4803	2.12	158.0905268
5.1	1.252	400	185	2.801428	1.905177	92.08	123.17	31.0871	2.12	189.553542
5.2	1.252	400	191	2.801428	1.935825	96.61	126.51	29.9068	2.98	198.3174904
5.3	1.252	400	181	2.801428	1.884468	96.61	125.92	29.3158	2.88	200.1221925
5.4	1.252	400	184	2.801428	1.900021	91.69	124.94	33.251	2.25	177.0236827
5.5	1.252	400	191	2.801428	1.935825	94.44	127.30	32.8581	2.78	180.5047012

A.3 Pencil-lead breaking method Calibration data of the MSI DT1-052K/L w/rivets PVDF sensor

Trail	lead type	Protruding lenght (mm)	block mass(g)	Water mass (g)	Total weight(N)	Duration (µs)	Pk-Pk	max (mV)	min(mV)	F(N)
1.1.20	HB	20	480	915	13.68495	8	185	114	-71	8.21097
1.2.20	HB	20	480	815	12.70395	11	167	118	-49	7.62237
1.3.20	HB	20	480	793	12.48813	9.5	141	106	-35	7.492878
1.4.20	HB	20	480	600	10.5948	7	123	74	-49	6.35688
1.5.20	HB	20	480	765	12.21345	7.2	205	102	-103	7.32807
1.6.20	HB	20	480	925	13.78305	6.5	159	108	-80	8.26983
1.7.20	HB	20	480	895	13.48875	8	175	112	63	8.09325
1.1.20	H	20	480	800	12.5568	6.6	169	113	-56	7.53408
1.2.20	H	20	480	940	13.9302	8.4	167	117	-50	8.35812
1.3.20	H	20	480	910	13.6359	9.8	167	95	-72	8.18154
1.4.20	H	20	480	915	13.68495	9.2	185	85	-100	8.21097
1.5.20	H	20	480	970	14.2245	8	173	60	-112	8.5347
1.6.20	H	20	480	965	14.17545	9.8	203	82	-121	8.50527
1.7.20	H	20	480	900	13.5378	8.7	172	66	-106	8.12268
1.1.15	H	15	480	1440	18.8352	4.8	209	87	-122	11.30112
1.6.15	H	15	480	1450	18.9333	5.8	203	101	-102	11.35998
1.2.15	H	15	480	1470	19.1295	5.5	182	83	-99	11.4777
1.3.15	H	15	480	1350	17.9523	6	214	92	-122	10.77138
1.4.15	H	15	480	1550	19.9143	8	166	63	-102	11.94858
1.5.15	H	15	480	1565	20.06145	7.4	193	73	-120	12.03687
1.7.15	H	15	480	1570	20.1105	5.5	205	89	-116	12.0663

A. 4 Pencil-lead breaking method Calibration data of the MSI DT1-028K/L w/rivets PVDF sensor

Trail	lead type	Protruding lenght (mm)	block mass(g)	Water mass (g)	Total weight(N)	Duration (µs)	Pk-Pk	max (mV)	min(mV)	F(N)
2.1.15	H	15	480	1380	22.51395	7.2	171	95	-76	13.50837
2.2.15	H	15	480	1400	22.71015	7.5	171	99	-72	13.62609
2..3.15	H	15	480	1480	23.49495	7.8	141	75	-72	14.09697
2.4.15	H	15	480	1245	21.1896	7.5	125	76	-48	12.71376

ITEM NO.	PART NUMBER	QTY.
1	base Plate	1
2	STRUT_PROFILE_40X40L.stp	2
3	sheet	1
4	L-angle	6
5	Block	1
6	BRACKET_40X40.stp	1
7	screw rod	1
8	ISO - 4032 - M8 - W - N	4
9	support_plate	1
10	ISO - 4035 - M8 - N	1
11	plate_sheet	1
12	wooden_block	1
13	wodden_place	1
14	wodden_2	1
15	sensor	1
16	lead	1
17	hook	1
18	ISO 4016 - M5 x 25 x 16-WN	8

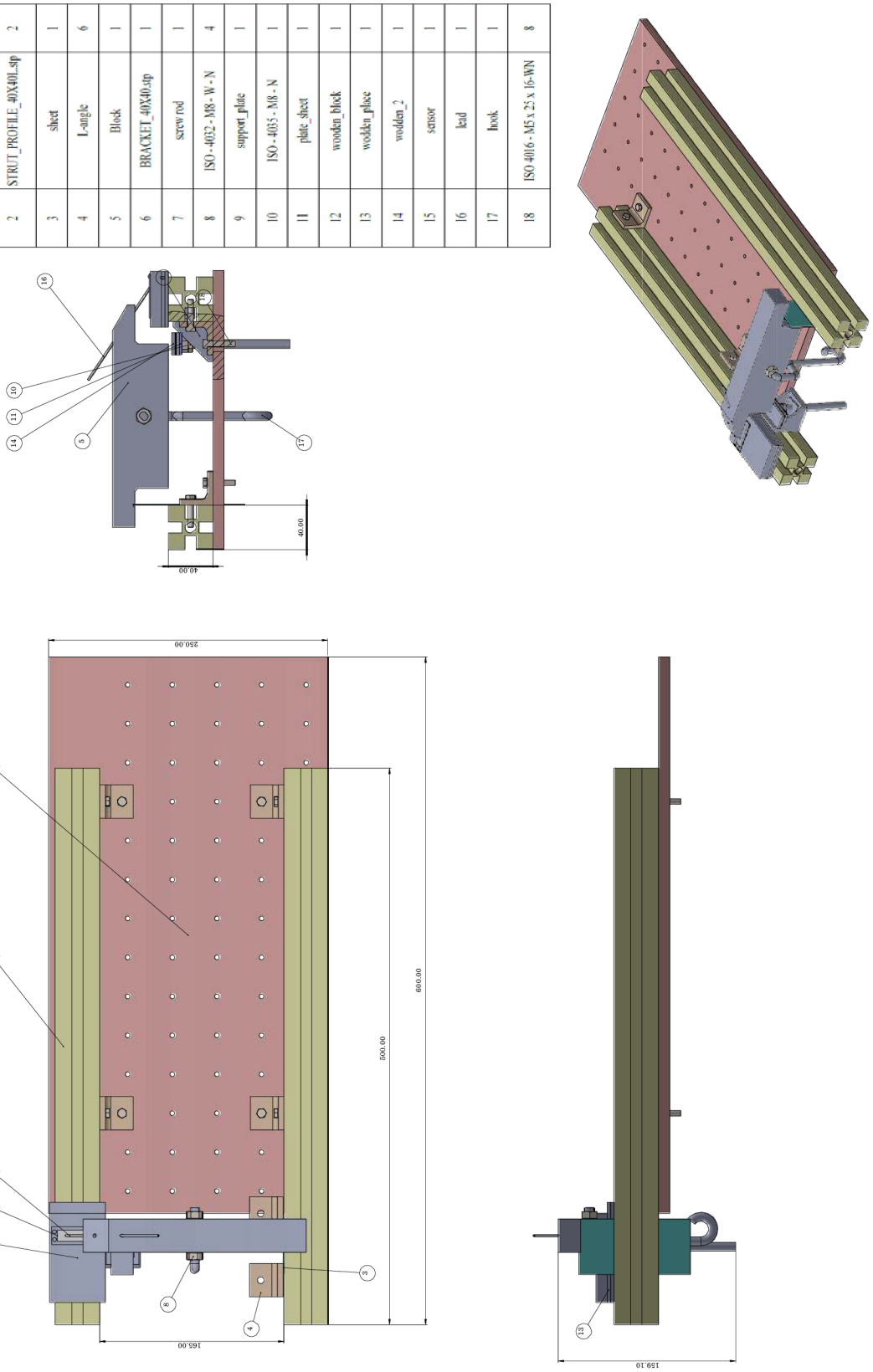

Figure A. 1 Pencil-lead breaking method Calibration apparatus

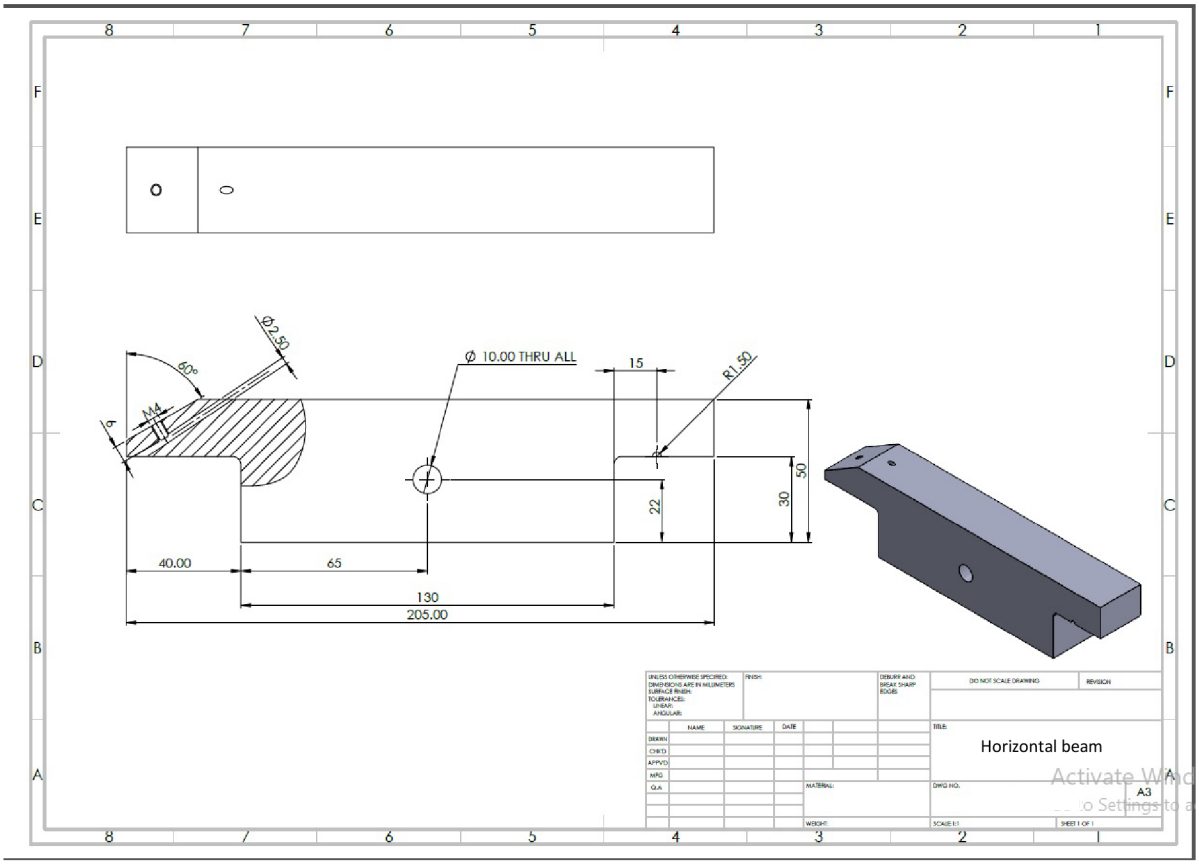

Figure A. 2 Horizontal Beam dimension